CALIFORNIA INSTITUTE OF TECHNOLOGY

CIT - ELECTRON TUBE & MICROWAVE
LABORATORY REPORT

DIRECTED ELECTRON VELOCITY DISTRIBUTIONS IN RARE GAS DISCHARGES USING GUARD RING PROBES

by

Robert H. Bond

Technical Report No. 25

Nonr 220(50)

June 1965

A REPORT ON RESEARCH CONDUCTED UNDER

CONTRACT WITH THE OFFICE OF NAVAL RESEARCH

DIRECTED ELECTRON VELOCITY DISTRIBUTIONS IN RARE GAS DISCHARGES USING GUARD RING PROBES

by

Robert H. Bond

Technical Report No. 25

CALIFORNIA INSTITUTE OF TECHNOLOGY
Pasadena, California

A Technical Report to the Office of Naval Research

Contract Nonr 220(50)

June 1965

ACKNOWLEDGEMENT

The author is deeply indebted to many people for their direct contributions to this project. In its initial stages the work was supported by the National Bureau of Standards, Boulder, Colorado. Particular thanks go to Frank Haller and John Trickey of that laboratory for their work in constructing the necessary equipment.

During the major portion of this work the interest and suggestions of Professors R. V. Langmuir and R. W. Gould proved invaluable. My hat is off to Howard Friedrich whose skill made it possible to construct the probe described here. Also, many thanks are due Fred Wild for his expert glass work. The major portion of this work was supported by the Office of Naval Research Contract Nonr 220(50). I.B.M. and the Hughes Aircraft Company have been most generous in their fellowship support of the author.

A special word of appreciation is due Mrs. Ruth Stratton for her skillful work in preparing the manuscript.

DIRECTED ELECTRON VELOCITY DISTRIBUTIONS IN RARE GAS DISCHARGES USING GUARD RING PROBES

Robert H. Bond

Abstract

An experimental technique for determining detailed properties of anisotropic electron velocity distributions is described. For a planar Langmuir probe it is shown that $g(v_z) = -\frac{m}{e^2}\frac{\partial J_p}{\partial V_p}$ where $v_z = \sqrt{2\frac{e}{m}V_p}$ and $g(v_z)$ gives the density of electrons with velocities normal to the probe in the range v_z to $v_z + dv_z$. This expression is valid for any distribution function making it possible to study anisotropies merely by changing the orientation of the probe. If the distribution function is isotropic the above expression is valid for cylindrical and small spherical probes as well.

This technique is applied to the measurement of the directional properties of electron velocity distributions in the positive column of neon and helium hot cathode discharges. The necessary planar probe consists of a 0.01 inch diameter circular probe surrounded by a 0.090 inch square guard-ring. The measured distributions were Druyvesteyn in form except that all electrons were shifted in energy (in the direction of the external field) by an amount proportional to $E\lambda(v_z)$. Here E is the magnitude of the external electric field and $\lambda(v_z)$ the electron mean free path as a function of v_z. The experimental conditions are shown to be identical with those necessary in the derivation of the Druyvesteyn distribution.

TABLE OF CONTENTS

I. INTRODUCTION

1.1 History of Problem

It is known that conducting probes were used by Crookes in the eighteen-nineties to explore ionized gases. Also, J. S. Townsend discussed the use of such probes in the early nineteen-hundreds. However, it was not until the work of Irving Langmuir in 1923 that the operation of these probes was understood. Langmuir presented his probe theory in a series of articles in the General Electric Review (1-5). In these articles Langmuir assumed that the plasma electrons had a Maxwellian energy distribution and with this assumption found that the current drawn by the probe as a function of negative probe potential is

$$I_p = K_1 e^{-aV_p} + K_2 \qquad (1.1)$$

Here K_1, K_2 and a are constants, while I_p is the electron current and V_p the absolute value of the probe potential with respect to the body of the plasma. Because of the exponential nature of this relationship it was (and still is) common practice to plot $\ell n\, I_p$ versus V_p. The constant a can then be determined from the linear plot. However, soon after Langmuir's publication, it became evident that many of the $\ell n\, I_p$ versus V_p plots were not linear (particularly if taken to sufficiently high values of V_p). Assuming that the

(1) I. Langmuir, H. Mott-Smith, General Electric Review 27, 449 (1924).
(2) Ibid. 538
(3) Ibid. 616
(4) Ibid. 762
(5) Ibid. 810

probes were functioning "properly" this means that the distribution functions were not Maxwellian as Langmuir assumed.

In 1930 Druyvesteyn (6) devised a scheme for overcoming this problem in the use of Langmuir probes. He developed a theory which showed that for planar, cylindrical, and small spherical probes the actual electron velocity distribution function could be obtained from the probe volt-ampere characteristic as follows:

$$f(v) = \frac{4mV_p}{A\,e^2}\frac{\partial^2 I_p}{\partial V_p^2} \qquad (1.2)$$

where $f(v)$ is the speed distribution of the electrons giving the number of electrons with speeds in the range v to $v+dv$, A is the collecting area of the probe, and m and e are the mass and charge of the electrons. The one major assumption necessary to arrive at the above result is that the distribution function is isotropic. Because it has become more and more evident that in many cases the electrons do not have a Maxwellian distribution, this technique for measuring distribution functions has gained increasing favor. At first the second derivatives of the probe curves were obtained graphically. This was quite unsatisfactory in that the original curves were subject to many errors and the graphical differentiation multiplied these errors to an intolerable point.

In 1934 (at the suggestion of K. G. Emeléus) R. H. Sloane and E. I. R. MacGregor (7) devised an ingenious method to overcome the need

---

(6) M. J. Druyvesteyn, Z. Physik 64, 781 (1930).

(7) R. H. Sloane, E.I.R. MacGregor, Phil.Mag.18, 193 (1934).

of graphical differentiation. Their technique involved superimposing a small a-c potential on the d-c probe potential. This causes the d-c probe current to increase over the value it would have with no a-c applied. The amount of increase is proportional to the second derivative of the probe characteristic. This can be understood by considering the Taylor series expansion of the probe current when the probe voltage has the form

$$V_p = V + e \quad \text{where} \quad e = A \cos \omega t \tag{1.3}$$

This gives

$$I_p = f(V_p) = f(V+e) = f(V) + ef'(V) + \frac{e^2}{2!} f''(V) + \cdots \tag{1.4}$$

On substituting for e this becomes

$$\begin{aligned} I_p = &\left\{ f(V) + \frac{A^2}{4} f''(V) + \frac{A^4}{64} f''''(V) + \cdots \right\} \\ &+ \left\{ Af'(V) + \frac{A^3}{8} f'''(V) + \cdots \right\} \cos \omega t \\ &+ \left\{ \frac{A^2}{4} f''(V) + \frac{A^4}{48} f''''(V) + \cdots \right\} \cos 2\omega t + \cdots \end{aligned} \tag{1.5}$$

which shows that for sufficiently small applied a-c voltages $[\frac{A^4}{64} f''''(V) \ll \frac{A^2}{4} f''(V)]$ the change in the d-c probe current is proportional to the second derivative of the probe curve.

This technique was used by Sloane and MacGregor (8) and later

(8) Ibid.

by Emeléus, Montgomery and Grieves (9), Emeléus and Ballentine (10) and Grieves and Johnston (11) to measure the velocity distributions in low pressure glow discharges. The work of these people in the field represents the most extensive work done until the early nineteen-fifties.

One other piece of work deserves mention. This is the technique developed by A. H. van Gorcum (12) in 1936. Van Gorcum again used a small a-c voltage applied to the probe, but he also devised a unique and ingenious bridge circuit which made it possible to determine the second derivative of the probe curves, point by point. It is probably because the technique was slow that it did not see greater use. Van Gorcum's circuit is shown in Figure 1.1. The following is a summary of his technique. The voltage appearing on the vertical plates of his oscilloscope was $g_2(V_y - \overline{V}_y)$ where $\overline{V}_y$ is the average value of V_y. The horizontal deflection was proportional to $g_1(V_p - \overline{V}_p)$. By Kirchhoff's voltage law we see that

$$V_y = k_1 I_p R - k_2 V_p \tag{1.6}$$

but $V_p = \overline{V}_p + K_p \cos \omega t$ and if we again expand $I_p = f(V_p)$ in a Taylor's series and substitute this into the above expression, we obtain

$$Y = a_o + a_1 X + a_2 X^2 + a_3 X^3 + \cdots$$

---

(9) K.G. Emeléus, F.D. Grieves, E. Montgomery, Proc.Roy.Irish Acad.A43, 35 (1936).
(10) K.G. Emeléus, R.J. Ballantine, Phys. Rev. 50, 672 (1936).
(11) F.D. Grieves, J.E. McF. Johnston, Phil. Mag. 21, 659 (1936).
(12) A.H. van Gorcum, Physica 3, 207 (1936).

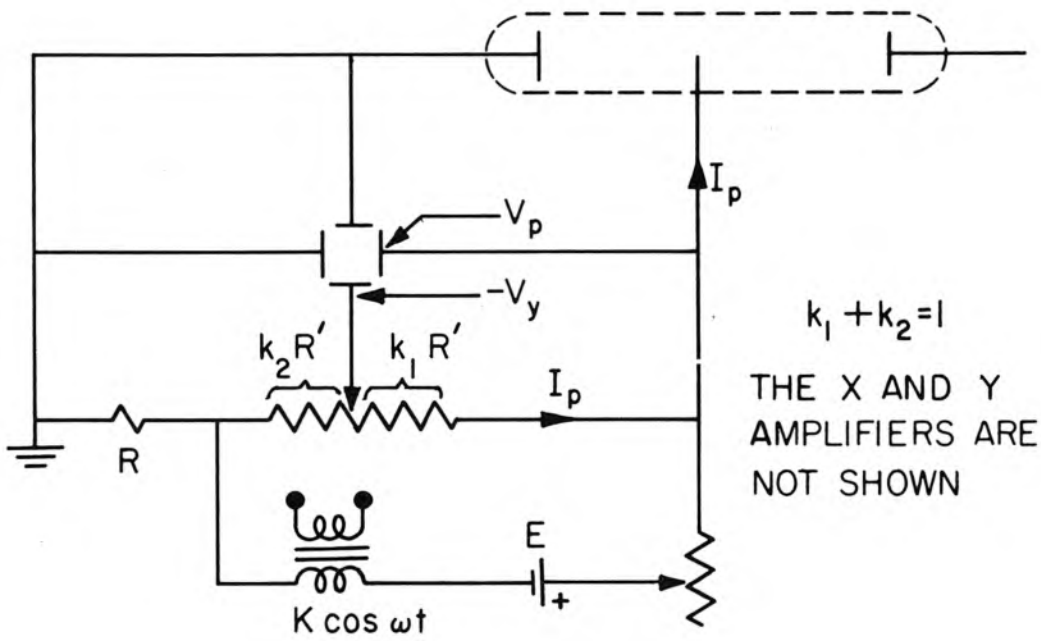

Fig. 1.1 A. H. van Gorcum's Circuit for Obtaining $\frac{d^2I_p}{dV_p^2}$

where $Y = g_2(V_y - \bar{V}_y)$, $X = g_1(V_p - \bar{V}_p)$

and

$$a_o = g_2(k_1 Rf - k_2 \bar{V}_p - \bar{V}_y)$$

$$a_1 = \frac{g_2}{g_1}(k_1 Rf' - k_2)$$

$$a_2 = \frac{g_2}{2g_1^2} k_1 Rf'' \qquad (1.7)$$

This is the equation of the curve plotted on the oscilloscope. We see that for sufficiently large g_1 only the first four terms of this series need be considered.

Van Gorcum adjusted k_1 and k_2 such that a_1 was zero, by noting when $\left.\frac{dY}{dX}\right|_{X=0} = 0$. Having done that, a_2 could be determined from the expression

$$a_2 = \frac{1}{2}\left\{Y(-1) + Y(+1) - 2Y(0)\right\} \qquad (1.8)$$

or

$$f'' = \frac{g_1^2}{g_2 k_1 R}\left\{Y(-1) + Y(+1) - 2Y(0)\right\} \qquad (1.9)$$

Using this technique van Gorcum studied distribution functions near the cathode in neon discharges.

In 1951 Kagan, Fedorov, Malyshev and Gavalles (13) swept the probe voltage linearly in time so that $\frac{d^2I_p}{dV_p^2}$ was proportional to $\frac{d^2I_p}{dt^2}$. They then obtained $\frac{d^2I_p}{dt^2}$ by using two R-C differentiating circuits. This method shows great promise in theory but is quite

(13) J.M. Kagan, V.L. Fedorov, G.M. Malyshev, L.A. Gavallas, Dokl.Akad. Nauk.SSSR 76, 215 (1951).

difficult to implement experimentally due to the inherent noise present in the plasmas being probed. It is speculated that for this reason the technique was dropped.

In 1953 Malyshev and Federov published a paper (14) in which they described an improvement on the Sloane and MacGregor technique. This consisted of superimposing a small sinusoidally modulated a-c voltage on the probe voltage such that the e of equation 1.3 becomes $A(1+\cos\omega_p t)\cos\omega t$. This leads to

$$I_p = f(V) + \frac{3}{8}A^2 f''(V) + \cdots + \left\{\frac{A^2}{2}f''(V) + \frac{7}{64}A^4 f''''(V) + \cdots\right\}\cos\omega_p t + \cdots \qquad (1.10)$$

Here we see that if A is sufficiently small, the component of the current at ω_p is proportional to $f''(V)$. Malyshev and Federov took advantage of this by building narrow band amplifiers tuned to ω_p . The output of these amplifiers is then proportional to $f''(V)$. The advantage over the Sloane and MacGregor technique is that here, assuming ideal filtering, the only error is due to neglecting the terms involving f'''', etc. which is quite valid for small A . With no modulation on the a-c voltage one must measure the change in the d-c probe current as the a-c is switched on and off. This is subject to large errors because very slight drifts in the d-c plasma conditions can cause $f(V)$ to vary the same order of magnitude as the quantity

---

(14) G.M. Malyshev, V.L. Federov, Dok.Akad.Nauk.SSSR 92, 269 (1953).

being measured [namely, $\frac{A^2}{4} f''(V)$] .

At nearly the same time (1954), R. L. F. Boyd and N. D. Twiddy (15) developed an almost identical technique. However, there were four major differences.

1. Boyd and Twiddy used square wave modulation instead of sinusoidal. This is of no consequence and merely changes the constants in the expansion of I_p .
2. Synchronous detection was used to select the current component at ω_p rather than narrow band amplifiers operating at ω_p .
3. A sensing probe was placed at a point near the measuring probe so that fluctuations in plasma potential could be measured. These fluctuations were then compensated for in the applied probe potential. Thus the probe tracked any plasma potential variations.
4. The small a-c signal was applied to the discharge rather than to the probe. This made it possible to keep the probe grounded.

The second of these differences merely exchanges filtering at low frequency for filtering at ω_p . It is felt that with easily obtainable equipment the synchronous detection scheme would yield a better signal to noise ratio.

The third point is an interesting attempt at taking into account the fluctuations which always occur in plasmas. Although it does not compensate for density changes, temperature changes, etc., it is a step in the right direction. It should be pointed out that even with

---

(15)R.L.F. Boyd, N.D. Twiddy, Nature 173, 633 (1954)

this type of compensation, probe curves taken in oscillating plasmas are not easily interpreted.

This technique for determining $\frac{d^2I_p}{dV_p^2}$ has been used by R.L.F. Boyd and N. D. Twiddy (16,17), N. D. Twiddy (18), J. B. Thompson (19) and N. D. Twiddy (20) to amass the most comprehensive set of measured distribution functions available.

In 1963 A. Garscadden and R. S. Palmer (21) developed a unique technique for obtaining the first derivative of the probe curve in a noise-free form. Because the signal was noise free, they were able to use R-C differentiation to obtain the second derivative. Two identical probes were used but they were biased at potentials differing by ΔV. A differential amplifier was used to measure the difference in the currents to the two probes. Since ΔV was held constant, the output of the differential amplifier was proportional to $\frac{\Delta I_p}{\Delta V_p} = \frac{dI_p}{dV_p}$. Because voltage fluctuations are well correlated over the distance between the probes, the noise output of the differential amplifier was found to be an order of magnitude less than the noise appearing on the individual probe curves. This technique is only valid in a plasma which is quite homogeneous because the basic assumption is that there is no variation in the plasma parameters over distances equal to the probe separation.

---

(16) R. L. F. Boyd, N. D. Twiddy, Proc. Roy. Soc. A250, 53 (1959).
(17) R. L. F. Boyd, N. D. Twiddy, Proc. Roy. Soc. A259, 145 (1960).
(18) N. D. Twiddy, Proc. Roy. Soc. A262, 379 (1961)
(19) J. B. Thompson, Proc. Roy. Soc. A262, 503 (1961)
(20) N. D. Twiddy, Proc. Roy. Soc. A275, 338 (1963).
(21) A. Garscadden, R. S. Palmer, Aeronautical Research Labs., USAF Report No. ARL63-50 (1963).

During this same period of time, G. R. Branner, E. M. Friar and G. Medicus (22) instrumented another technique for determining the second derivative of a probe characteristic. They also superimposed a small a-c voltage on the probe, but instead of noting the change in d-c current they detected the second harmonic probe current. Equation 1.5 shows that for a small a-c potential this frequency component of the probe current is proportional to $\frac{d^2I_p}{dV_p^2}$. The second harmonic current was measured using band pass filtering and synchronous detection. The instrumentation necessary for this technique is much simpler than that necessary when using modulated a-c and the accuracy of this system seems to be as good, making this a very promising technique.

1.2 Object of This Experiment

The work presented here was first discussed by the author in a paper presented in 1962 (23). At that time it was shown that for a planar probe the first derivative of probe current with respect to probe voltage is proportional to $g(v_z)$. Here $g(v_z)$ is the directed electron velocity distribution giving the density of electrons with z directed velocities in the range v_z to $v_z + dv_z$. The derivation of this result is given in Section 2.3. The most important point in this derivation is that it is not necessary to assume that the distribution function is isotropic. It was also shown in the previous paper that a guard-ring probe could be constructed such that it exhibited planar geometry.

---

(22) G. R. Branner, E. M. Friar, G. Medicus, Rev. Sci. Instr. 34, 231 (1963)

(23) R. H. Bond, Bull. Am. Phys. Soc. 7, 631 (1962).

This thesis extends the above theory to show that if the distribution function is isotropic the first derivative of the probe curve is proportional to $g(v_z)$ for cylindrical and small spherical probes as well as planar probes. The advantage in using planar probes is that it is then possible to measure any anisotropy of the electron distribution.

The experiments described here use a guard ring probe to measure (for the first time) the detailed directional properties of electron distributions. The plasma probed is the positive column of neon and helium hot cathode discharges. These experimental distributions are then compared with theoretical distributions calculated for plasma conditions similar to the experimental conditions. Since it was only necessary to obtain the first derivative in this work, the probe voltage was swept linearly in time and the time derivative obtained using an operational amplifier.

Section 2.2 presents the solution of the Boltzmann equation under conditions applicable to the experiments described here. This leads to the theoretical distribution functions which are later compared (Sections 4.3 and 4.4) with experimental results. Sections 2.3 and 2.4 discuss the theory behind the application of probes to electron distribution measurement.

Chapter III describes the experiment and experimental apparatus, while Chapter IV discusses the results obtained. Finally, Chapter V consists of conclusions and recommendations for further work.

II. THEORY

2.1 Introduction

This section will be divided into two main parts. The first of these will deal with the solution of Boltzmann's equation under conditions in which we are interested. This analysis yields the electron velocity distribution in terms of an expansion in Legendre polynomials in velocity space. The remainder of the section deals with the theory involved in experimentally verifying (or refuting) this distribution function. This second section can again be divided into that portion dealing generally with measurement of velocity distribution using probes, and a portion looking more closely at the technique actually used for these experiments.

MKS units are used except where it is specifically indicated otherwise.

2.2 Solution of Boltzmann's Equation

As stated previously, we are interested in measuring the directed velocity distributions of electrons in rare gas discharges. We will see (a posteriori) that the plasma used in the experiments described here has the following properties. First, it is very weakly ionized (of the order of 10^{-4}%) so that the dominant interactions or collisions between particles are those between electrons and neutrals. This allows us to neglect electron-electron and electron-ion collision terms in the Boltzmann equation. Second, in the positive column of the discharge there exists a relatively high electric field directed along

the axis of the tube. Since there is no magnetic field applied, this electric field will be assumed to produce the only external force on the electrons. We will further assume that the distribution function has reached a steady state condition and is spatially homogeneous. Picking a coordinate system with the z axis along the axis of the tube (in the direction of the electric field E), we arrive at the following form for Boltzmann's equation:

$$-\frac{eE}{m}\frac{\partial f}{\partial v_z} = \left.\frac{\partial f}{\partial t}\right|_{\text{collisions}} \tag{2.1}$$

Here f is the distribution function for the electrons. That is, $f(v)\,\underline{dv}$ gives the density of electrons with velocities within $\underline{dv} = dv_z dv_y dv_z$, E is the magnitude of the electric field, e is the electronic charge, m is the electronic mass, v_z is the z-directed electron velocity, and $\left.\frac{\partial f}{\partial t}\right|_{\text{collision}}$ is the time rate of change of the distribution function due to collisions. This collision term can be written in many ways; however, we will write it in the form derived by Chapman and Cowling (1) and others. This gives

$$\left.\frac{\partial f}{\partial t}\right|_{\text{collisions}} = \int_{\Omega}\int_{\underline{dv}} [f(v')\,F(v') - f(v)\,F(v)]\,u\sigma d\Omega\,\underline{dv} \tag{2.2}$$

where f is as defined previously and F is the distribution function for the particles with which the electrons collide (in this case, neutral gas molecules). Primes denote velocities after a collision

---

(1) S. Chapman, T.G. Cowling, The Mathematical Theory of Non-Uniform Gases (Cambridge University Press, 1953), pp. 54-65.

while unprimed quantities indicate initial velocities. V will be used to denote neutral velocities, while v represents electron velocities. The quantity u is the magnitude of the difference in velocity of the particles before collision; $u = |\underline{v} - \underline{V}|$. The quantity $\sigma(\Theta,u,\emptyset)d\Omega = \sigma(\Theta,u,\emptyset)\sin\Theta d\Theta d\emptyset$ is just the function relating the number of electrons per second scattered into solid angle $d\Omega$ by a single scattering center to the flux of electrons arriving per sec per m^2 at the scattering center with relative velocity u,

$$\text{i.e.,} \quad \frac{dN_{out}}{dt} = \sigma(\Theta,u,\emptyset)\, d\Omega \frac{dN_{in}}{dt} \tag{2.3}$$

Figure 2.1 shows the angles Θ and $\emptyset$ measured in a coordinate system moving with the scattering center. The expression is integrated over all scattering angles $(d\Omega)$ and over all initial scatterer velocities $\underline{dV} = dV_x dV_y dV_z$. This form for the collision term is valid under the assumptions of binary, elastic, short-term collisions--collisions in which no energy goes to excite internal degrees of freedom in the colliding bodies and the collision takes place in a time interval short compared with dt . This rules out collisions where excitation or ionization takes place. Electron-electron and ion-electron collisions must also be ruled out because the forces involved in these cases are long range and involve interaction times long compared to dt . In addition, these collisions are not strictly binary. A review of Chapman and Cowling's derivation of this form of the collision term is presented in Appendix A.

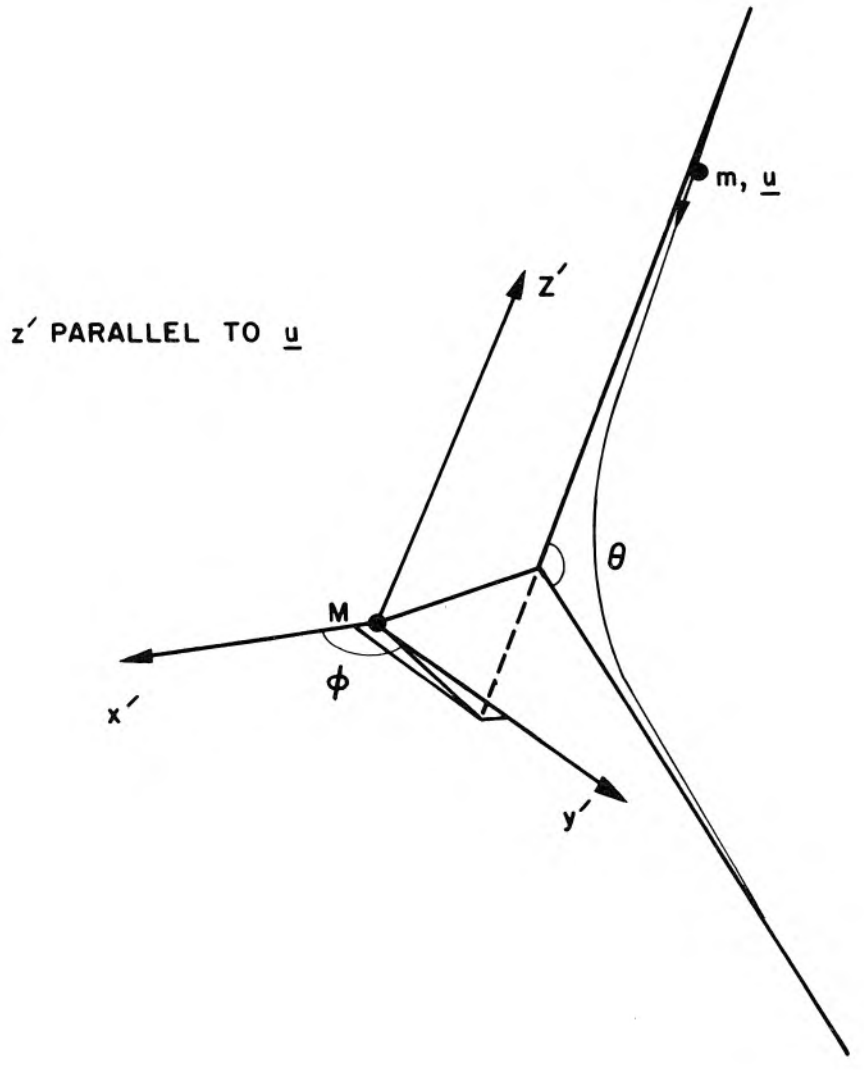

Fig. 2.1 Collision Geometry in Frame Moving with Scatterer

Inserting this form for the collision term, Boltzmann's equation becomes

$$-\frac{eE}{m}\frac{\partial f}{\partial v_z} = \int_{\Omega}\int_{\underline{dV}} [f(v')\,F(V') - f(v)\,f(V)]\,u\sigma\,d\Omega\,\underline{dV} \qquad (2.4)$$

We will solve this equation by expanding f in a series of Legendre polynomials (2) giving

$$f = \sum_{\ell} f_{\ell}(v)\,P_{\ell}(\cos\Theta_1) \qquad (2.5)$$

where Θ_1 is the angle between $\underline{v}$ and the z axis, or alternatively, the angle between $\underline{v}$ and $\underline{E}$. Substituting this expression into the Boltzmann equation, multiplying by $P_i(\cos\Theta_1)$, and integrating over $d\Omega$, we obtain

$$-\int P_i(\cos\Theta_1)\,\frac{eE}{m}\,\frac{\partial}{\partial v_z}\sum_{\ell} f_{\ell}P_{\ell}(\cos\Theta_1)\,d\Omega_1 =$$

$$\int P_i(\cos\Theta_1)\,S\,d\Omega_1 \qquad (2.6)$$

where S has been substituted for the collision term. Since the f_{ℓ}'s are explicit functions of v, not v_z, we use the relationships $v_z = v\cos\Theta_1$ and $v^2 = v_x^2 + v_y^2 + v_z^2$ to show that

$$\frac{\partial}{\partial v_z}\left\{f_{\ell}\,P_{\ell}(\cos\Theta_1)\right\} = P_{\ell}(\cos\Theta_1)\cos\Theta_1\frac{\partial f_{\ell}}{\partial v} + \frac{f_{\ell}\sin^2\Theta_1}{v}\frac{\partial P_{\ell}}{\partial(\cos\Theta_1)} \qquad (2.7)$$

---

(2) W. P. Allis, Vol.XXI Handbuch der Physik, Ed, S. Flügge (Springer-Verlag, Berlin 1956), pp. 404-406.

Making use of this and the following well-known properties of Legendre polynomials:

$$(2\ell+1)\cos\theta_1 P_\ell = (\ell+1)P_{\ell+1} + \ell P_{\ell-1}$$

$$(2\ell+1)\sin^2\theta_1 \frac{\partial P_\ell}{\partial(\cos\theta_1)} = \ell(\ell+1)\left[P_{\ell-1} - P_{\ell+1}\right]$$

$$(2\ell+1)\int P_\ell P_m d\Omega_1 = 4\pi\,\delta_{\ell m} \tag{2.8}$$

we obtain

$$-\frac{eE}{m}\sum_\ell \int d\Omega_1 P_i \left\{\left[\frac{(\ell+1)P_{\ell+1} + \ell P_{\ell-1}}{2\ell+1}\right]\frac{\partial f_\ell}{\partial v} + \frac{\ell(\ell+1)}{2\ell+1)}\left[P_{\ell-1} - P_{\ell+1}\right]\frac{f_\ell}{v}\right\}$$

$$= \int P_i S\, d\Omega_1 = S_i \frac{4\pi}{2i+1} \tag{2.9}$$

where we have now expanded the collision term in a series of Legendre polynomials, i.e.,

$$S = \sum_i S_i P_i(\cos\theta_1) \tag{2.10}$$

We obtain a single equation for each value of i substituted into 2.9. The first two of these are

$$S_o = \frac{-eE}{m}\left\{\frac{1}{3}\frac{\partial f_1}{\partial v} + \frac{2}{3}\frac{f_1}{v}\right\} = \frac{-eE}{3mv^2}\frac{\partial(v^2 f_1)}{\partial v} \tag{2.11}$$

$$S_1 = \frac{-eE}{m}\left\{\frac{\partial f_o}{\partial v} + \frac{2}{5}\frac{\partial f_2}{\partial v} + \frac{6}{5}\frac{f_2}{v}\right\} = \frac{-eE}{m}\left\{\frac{\partial f_o}{\partial v} + \frac{2}{5v^3}\frac{\partial(v^3 f_2)}{\partial v}\right\} \tag{2.12}$$

V. L. Ginzburg shows (3) that in the second of these equations the term involving f_2 can be neglected. In particular he shows that the condition $\frac{\partial f_o}{\partial v} \gg \frac{1}{v^3}\frac{\partial (v^3 f_2)}{\partial v}$ reduces to $\frac{m}{M} \ll 1$ where M is the mass of the scatterer and m the mass of the scattered particle. Since we are talking about electron-neutral scattering, this condition is met and equations 2.11 and 2.12 reduce to two equations for f_o and f_1. We will assume that all higher order terms f_2, f_3, f_4, etc. are negligible and that the distribution function can be written

$$f(v,\theta_1) = f_o(v) + \cos\theta_1 f_1(v) \tag{2.13}$$

The validity of dropping the higher order terms is discussed by Ginzburg (4).

It would be well to note what the terms f_o and f_1 represent physically. The first term $f_o(v)$ represents an isotropic distribution whereas the second term $\cos\theta_1 f_1(v)$ represents an anisotropy which we will see can be interpreted as a drift velocity in the direction of the applied force on the electrons.

To solve the two equations, 2.11 and 2.12, it is necessary to determine S_o and S_1. In Appendix B it is shown that the S_o equation is directly related to an energy balance equation, while the S_1 equation represents the balance of z directed electron momentum. We would therefore expect S_o to be a strong function of the change in energy (Δv) of an electron during a collision. On the other hand,

(3)V. L. Ginzburg, A. V. Gurevich, Usp. Fiz. Nauk.70, 201 (1960)
(4) Ibid.

the change in the z directed momentum can be approximated very well by setting $\Delta v = 0$ and merely considering the change in direction of the electron. This is true because we are discussing the case of relatively heavy scatterers so that very little energy is transferred to them during a single collision. With these facts in mind let us write down an expression for S_i . From equations 2.9 and 2.2 this is

$$S_i = \frac{2i+1}{4\pi} \int d\Omega_1 P_i \iint d\Omega \underline{dV} u\sigma \, [f(v') \, F(V') - f(v) \, F(V)]$$

or

$$S_i = \frac{2i+1}{4\pi} \int d\Omega_1 P_i(\cos \Theta_1) \iint d\,\Omega \underline{dV} u\sigma \left\{ F(V') \sum_\ell f_\ell(v') P_\ell(\cos \Theta_1') - F(V) \sum_\ell f_\ell(v) \, P_\ell(\cos \Theta_1) \right\} \tag{2.14}$$

Noting the collision geometry as shown in Figure 2.2, again with the coordinates moving with the scatterer, we see that $\cos \Theta_1' = \sin \Theta_1 \sin \Theta \cos \phi_1 + \cos \Theta_1 \cos \Theta$ so in the expression for S_i we have terms of the form

$$P_\ell(\cos \Theta_1 \cos \Theta + \sin \Theta_1 \sin \Theta \cos \phi_1)$$

$$= P_\ell(\cos \Theta) \, P_\ell(\cos \Theta_1) + 2 \sum_{k=1}^{\ell} \frac{(\ell-k)!}{(\ell+k)!} P_\ell^k(\cos \Theta_1) P_\ell^k(\cos \Theta) \cos k\phi_1$$

see reference (5).

---

(5) P. M. Morse, H. Feshbach, Methods of Theoretical Physics--Part II (McGraw-Hill Book Company, Inc., New York 1953) p. 1327.

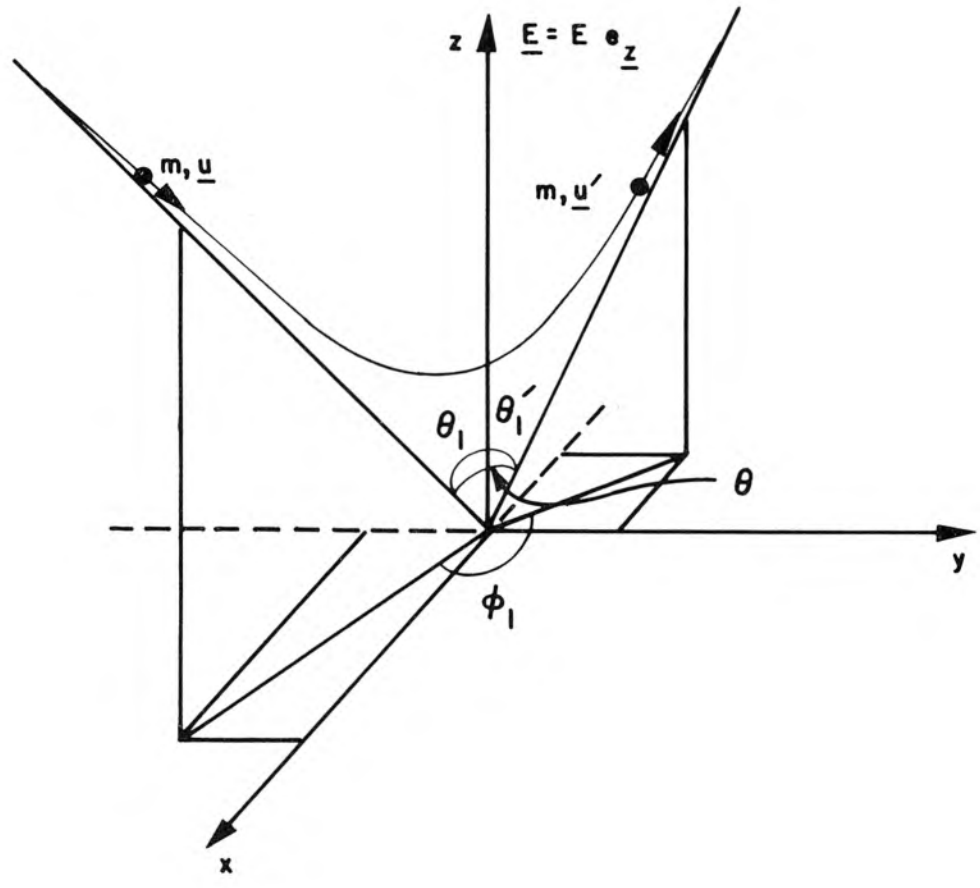

Fig. 2.2 Collision Geometry Defining Θ, Θ_1, Θ_1', and ϕ_1

All the terms containing $\cos k\phi_1$ will yield zero when integrated over $d\Omega_1$ so we are left with the following:

$$S_i = \iint d\Omega \underline{dV} u\sigma(u,\theta) \left\{ F(V')f_i(v')P_i(\cos\theta) - F(V)f(v) \right\} \qquad (2.15)$$

We will now apply the assumptions that the energy lost per collision is small (i.e., $v \cong v'$ and $V \cong V'$) and that $u \cong v$. The latter comes from assuming that the energies of the neutrals and electrons are comparable so that $V \ll v$ and therefore $u = |\overline{v} - \overline{V}| \approx v$. This gives

$$S_i = \iint d\Omega \underline{dV} v\sigma(v,\theta)\, F(V)\, f_i(v)[P_i(\cos\theta) - 1]$$

or

$$S_i = Nf_i v \int \sigma(v,\theta)[P_i(\cos\theta) - 1]\, d\Omega = -f_i \nu_i \qquad (2.16)$$

N is the density of the neutrals and ν_i are collision frequencies defined by

$$\nu_i = Nv \int \sigma(v,\theta)[1 - P_i(\cos\theta)]\, d\Omega \qquad (2.17)$$

As expected S_o is zero in this approximation.

It is necessary to look at the collision in some detail to determine S_o. This has been done by Desloge and Matthysse (6) for the case we are interested in. They assumed that the gas molecules were not affected by the electric field and had a Maxwellian distribution, i.e.,

---

(6) E. A. Desloge, S. W. Matthysse, Amer.Jour.Phys.28, 1 (1960)

$$F = \left(\frac{M}{2\pi\ kT}\right)^{3/2} Ne^{-\frac{MV^2}{2kT}}$$

where T is the gas temperature and k is Boltzmann's constant.

They find the same value for S_1 as given by 2.17 and

$$S_o = \frac{1}{2v^2}\frac{\partial}{\partial v}\left\{\frac{2mv^2\nu_1}{M}\left[\frac{kT}{m}\frac{\partial f_o}{\partial v} + vf_o\right]\right\} \tag{2.18}$$

Substituting these values of S_1 and S_o into 2.11 and 2.12 we obtain

$$-\frac{eE}{3mv^2}\frac{\partial(v^2 f_1)}{\partial v} = \frac{1}{2v^2}\frac{\partial}{\partial v}\left\{\frac{2mv^2\nu_1}{M}\left[\frac{kT}{m}\frac{\partial f_o}{\partial v} + vf_o\right]\right\} \tag{2.19}$$

$$-\frac{eE}{m}\frac{\partial f_o}{\partial v} = -\nu_1 f_1 \tag{2.20}$$

Multiplying 2.19 by v^2 and integrating from 0 to v gives

$$-\frac{eE}{3m}v^2 f_1 = \frac{v^2 m\nu_1}{M}\left[\frac{kT}{m}\frac{\partial f_o}{\partial v} + vf_o\right] \tag{2.21}$$

We can now substitute 2.20 into 2.21 and solve for f_o. This leads to

$$f_o = A\, e^{-\int^{v}\frac{mv\ dv}{kT + \frac{e^2E^2M}{3m^2\nu_1^2}}} \tag{2.22}$$

For $kT \gg \frac{e^2E^2M}{3m^2\nu_1^2}$ we obtain a Maxwellian distribution $f_o = Ae^{-\frac{mv^2}{2kT}}$.

However, if the electric field is "strong" such that $\frac{e^2E^2M}{3m^2\nu_1^2} \gg kT$, the distribution will in general not be Maxwellian. It is impossible to evaluate its exact form in this case unless we know ν_1 as a function

of v. One reasonable assumption is that the mean free path (λ) be independent of v. This leads to $\nu_1 = \frac{v}{\lambda}$, and for this condition we have

$$f_o = A\, e^{-\frac{3m^3v^4}{4\lambda^2e^2E^2M}} = A\, e^{-h^4v^4} \tag{2.23}$$

This is the Druyvesteyn distribution first derived by Druyvesteyn in 1930 (7).

The above function can be put in a more concise form by using as parameters the energy gained by the electrons per mean free path (in the direction of the field) and the electron energy. These will be denoted respectively as $W_\lambda = eE\lambda$ and $W = \frac{1}{2}mv^2$. Using these quantities we can write

$$f_o = A\, e^{-\frac{3m}{M}\left(\frac{W}{W_\lambda}\right)^2} = A\, e^{-h^4v^4} \tag{2.24}$$

so

$$h^4 = \frac{3m^3}{4M\,W_\lambda^2} \tag{2.25}$$

From 2.20

$$f_1 = -6\,\frac{m}{M}\left(\frac{W}{W_\lambda}\right) f_o \tag{2.26}$$

giving

$$f = f_o + \cos\theta_1 f_1 = A\left\{1 - \frac{6mW}{MW_\lambda}\cos\theta_1\right\} e^{-\frac{3m}{M}\left(\frac{W}{W_\lambda}\right)^2} \tag{2.27}$$

---

(7) M. J. Druyvesteyn, Physica 10, 69 (1930)

The "strong field" condition can be written as

$$\frac{W_\lambda^2 M}{6m W} \gg kT \tag{2.28}$$

The constant A will now be evaluated by noting that the integral of f over all velocities gives the electron density n, i.e.,

$$n = \int_0^\infty dv \int_0^{2\pi} d\phi \int_0^\pi d\theta_1 \left\{ A\left[1 - 3 \frac{m^2 v^2}{M W_\lambda} \cos\theta_1 \right] e^{-h^4 v^4} v^2 \sin\theta_1 \right\}$$

This yields

$$A = \frac{n h^3}{\pi \Gamma(\frac{3}{4})} \tag{2.29}$$

We can now calculate the mean energy $\frac{1}{2}\overline{mv^2}$ and the mean value of the z velocity $\overline{v_z}$. The latter will be termed the drift velocity. The mean energy is given by

$$\frac{m}{2n}\int v^2 f \, \underline{dv} = \frac{2mh^3}{\Gamma(\frac{3}{4})} \int_0^\infty v^4 e^{-h^4 v^4} dv = \frac{m\Gamma(\frac{5}{4})}{2h^2\Gamma(\frac{3}{4})}$$

or

$$\overline{\frac{1}{2} mv^2} = \overline{W} = \frac{m\Gamma(\frac{5}{4})}{2h^2\Gamma(\frac{3}{4})} = \sqrt{\frac{M}{3m}} \frac{\Gamma(\frac{5}{4})}{\Gamma(\frac{3}{4})} W_\lambda \tag{2.30}$$

In the same way we obtain $\overline{v_z}$.

$$\overline{v_z} = \frac{1}{n}\int v_z f \, \underline{dv} = -\sqrt{\frac{m\pi}{3M}} \frac{1}{h\Gamma(\frac{3}{4})} = \frac{-\sqrt{2\pi}\, W_\lambda^{1/2}}{\Gamma(\frac{3}{4})[3mM]^{1/4}} \tag{2.31}$$

Since directed distributions $g(v_x)$, $g(v_y)$, $g(v_z)$ were measured, we

will now calculate these functions so that the theory and experiment can be compared.

Let us first calculate $g(v_z)$. This function gives the density of electrons with z directed velocities in the range v_z to v_z+dv_z irrespective of their x or y velocities. Therefore $g(v_z)$ can be found by integrating $f(v)$ over all possible v_x and v_y. This yields

$$g(v_z) = A \int_{-\infty}^{\infty}\int e^{-h^4(v_x^2+v_y^2+v_z^2)^2} \left\{1-\frac{3m^2v_z}{MW_\lambda}\sqrt{v_x^2+v_y^2+v_z^2}\right\} dv_x dv_y \tag{2.32}$$

or in terms of polar coordinates $(r^2 = v_x^2 + v_y^2)$

$$g(v_z) = 2\pi A \int_0^{\infty} e^{-h^4(r^2+v_z^2)^2} \left\{1-\frac{3m^2v_z}{MW_\lambda}\sqrt{r^2+v_z^2}\right\} rdr \tag{2.33}$$

It is seen from this equation that for sufficiently large v_z the term arising from f_1 will dominate. We show in Appendix C that this does not happen for small enough energy to be of interest. Therefore we may ignore this second term except for calculating the drift velocity. That is, we have a nearly isotropic distribution with a superimposed drift.

Integrating the first term of 2.32 yields

$$g(v_z) \cong \frac{\sqrt{\pi}\, nh}{2\Gamma(\frac{3}{4})}\left\{1 - \mathrm{erf}(h^2v_z^2)\right\} \tag{2.34}$$

where erf is the error function defined by

$$\operatorname{erf} x = \frac{2}{\sqrt{\pi}} \int_0^x e^{-t^2}\, dt$$

The other two directed distribution functions can be calculated in the same fashion. They will both entail an integration over all v_z. From equation 2.32 we see that the term due to f_1 will be zero and both $g(v_x)$ and $g(v_y)$ will be given exactly by equation 2.34.

We can approximate the error function for large argument by the following asymptotic series: (8)

$$\operatorname{erf}(x) \cong 1 - \frac{e^{-x^2}}{\sqrt{\pi}\, x} \left\{ 1 - \frac{1}{2x^2} + \frac{1 \cdot 3}{2^2 x^4} - \cdots \right\}$$

This gives

$$g(v_z) \cong \frac{n}{2h\Gamma(\frac{3}{4})} \cdot \frac{e^{-h^4 v_z^4}}{v_z^2} \left\{ 1 - \frac{1}{2h^4 v_z^4} \cdots \right\} \quad \text{large } hv_z \tag{2.35}$$

For small hv_z we can expand the error function in a power series (9) giving

$$g(v_z) = \frac{\sqrt{\pi}\, nh}{2\Gamma(\frac{3}{4})} \left\{ 1 - \frac{2h^2 v_z^2}{\sqrt{\pi}} \left[1 - \frac{(h^2 v_z^2)^2}{3} + \cdots \right] \right\} \quad \text{small } hv_z \tag{2.36}$$

We see that for large v_z the directed distributions fall off very rapidly, going as $K \frac{e^{-h^4 v_z^4}}{v_z^2}$. While for small v_z they vary

(8) H. B. Dwight, Tables of Integrals and Other Mathematical Data, (The MacMillan Co., New York, 1957) p. 129.

(9) Ibid.

quadratically with v_z .

Summarizing the above theory we see that the electron distribution function should be Druyvesteyn rather than Maxwellian if

1. The degree of ionization is low so that only electron-neutral collisions need be considered.
2. The external electric field is strong, i.e.,

$$\frac{e^2E^2M}{3m^2\nu_1^2} \gg kT$$

3. The mean free path is independent of velocity so that

$$\nu_1 = \frac{v}{\lambda}$$

4. We ignore inelastic collisions.

Having derived this form for the distribution function it would be interesting to compare it with a Maxwellian one with the same electron density and mean energy.

We would like to compare

$$\text{Maxwellian} \quad g(v_z) = n\left(\frac{m}{2kT_e\pi}\right)^{1/2} e^{-\frac{mv_z^2}{2kT_e}} \tag{2.37}$$

$$\text{Druyvesteyn} \quad g(v_z) = n\,\frac{\sqrt{\pi}\,h}{2\Gamma(\frac{3}{4})}\left\{1 - \operatorname{erf}(h^2v_z^2)\right\} \tag{2.38}$$

$$\text{where} \quad \frac{3}{2}kT_e = \frac{m\Gamma(\frac{5}{4})}{2h^2\Gamma(\frac{3}{4})} \tag{2.39}$$

Setting $\frac{m}{2kT_e}v_z^2$ equal to the dimensionless variable x^2 and normalizing the Maxwellian distribution so that its maximum amplitude

is 1 , we obtain

$$\text{Maxwellian} \quad g(x) = e^{-x^2} \tag{2.40}$$

$$\text{Druyvesteyn} \quad g(x) = \frac{\pi}{\Gamma(\frac{3}{4})} \sqrt{\frac{\Gamma(\frac{5}{4})}{6\Gamma(\frac{3}{4})}} \left\{1 - \text{erf}\left[\frac{\Gamma(\frac{5}{4})}{2\Gamma(\frac{7}{4})} x^2\right]\right\} \tag{2.41}$$

$$= 0.90 \left\{1 - \text{erf}(0.493x^2)\right\}$$

These two functions are plotted in Figure 2.3. We see that the Druyvestyn distribution contains fewer low and high energy electrons. That is, the electron velocities have less spread about the mean for the Druyvesteyn case.

2.3 Measurement of Distribution Functions Using Probes

The preceding discussion demonstrates that from a theoretical point of view there is no reason to expect a slightly ionized gas always to have a Maxwellian velocity distribution. For this reason it is interesting to measure the distribution functions for various experimental conditions in order to determine what distribution actually exists. With this end in mind we will now discuss the theory of Langmuir probes and its application to the measurement of distribution functions.

Let us look at the volt-ampere characteristic of a planar probe (an infinite plane conductor in a semi-infinite plasma). We will assume the following conditions:

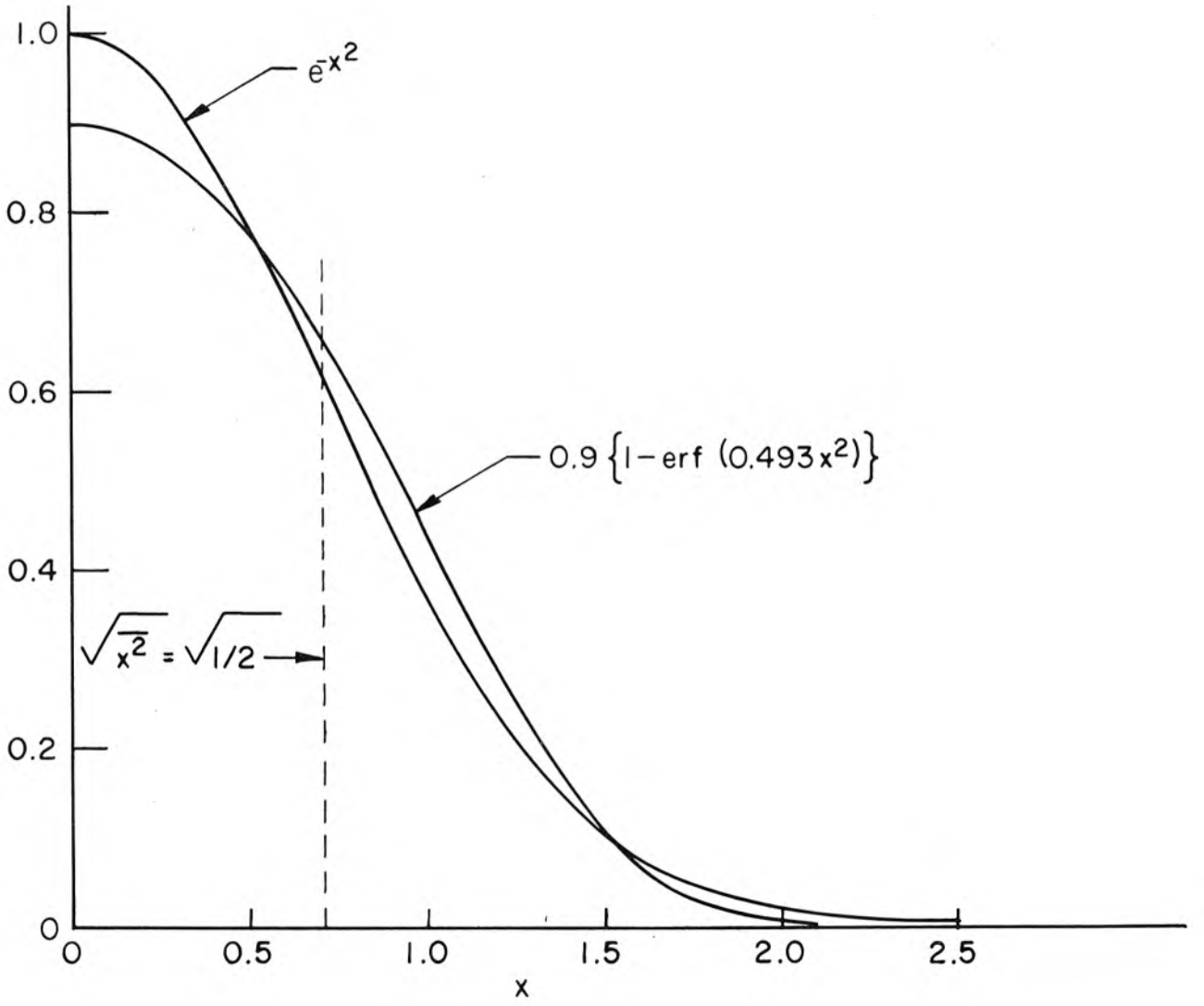

Fig. 2.3 Comparison of Maxwellian and Druyvesteyn Distributions with Same Density and Mean Energy

1. The probe is negative with respect to the plasma so that a sheath of positive charge covers the probe surface.
2. The electrons undergo no collisions in the sheath. That is, λ is much greater than the sheath thickness.
3. No electrons are produced in the sheath (including the probe surface). This means we neglect all ionization in the sheath, secondary electrons, photoemission, etc.
4. v_z represents electron velocities normal to the probe surface. This convention will be followed from this point on.

For this case the differential current density to the probe due to electrons in the velocity class v_z to v_z+dv_z is merely

$$|dJ_e(v_z)| = edn(v_z)\, v_z = v_z eg(v_z)\, dv_z \tag{2.42}$$

where $dn(v_z)$ is the density of electrons in the velocity range v_z to v_z+dv_z. Therefore

$$|J_e| = \int_{\substack{\text{all} \\ \text{possible} \\ v_z}} dJ(v_z) \tag{2.43}$$

The limits on v_z are determined from energy considerations. That is, the electrons must possess sufficient energy normal to the probe to overcome the negative probe potential ($\frac{1}{2} mv_z^2 \geq eV_p$). V_p is the absolute value of the probe potential with respect to the plasma potential. Plasma potential is the potential at the probe location with the probe

removed. Thus we have for the electron current density to the probe

$$|J_e| = \int_{\sqrt{2\frac{e}{m}V_p}}^{\infty} e\, v_z g(v_z)\, dv_z \tag{2.44}$$

The ion current is determined in exactly the same way. The only difference is that for negative probe potentials the ions have no potential hill to overcome and therefore all ions moving toward the probe are collected. Thus the ion current density to the probe is

$$|J_i| = \int_0^{\infty} e\, v_z F_i(v_z)\, dv_z \tag{2.45}$$

$F_i(v_z)$ is the distribution function for ions, giving the density of ions with velocities in the range v_z to v_z+dv_z.

We will call electron current to the probe positive so that for the total current density to the probe we have

$$J_p = |J_e| - |J_i| = \int_{\sqrt{2\frac{e}{m}V_p}}^{\infty} e\, v_z g(v_z)\, dv_z - \int_0^{\infty} e v_z F_i(v_z)\, dv_z \tag{2.46}$$

If both the ions and the electrons have Maxwellian velocity distributions this leads to

$$J_p = -eN_i \sqrt{\frac{kT_i}{2\pi M}} + en\sqrt{\frac{kT_e}{2\pi m}}\, e^{-\frac{eV_p}{kT_e}} \tag{2.47}$$

This is the commonly seen form for the volt-ampere relation of a Langmuir probe. If it is applicable, a plot of $\ell n(J_p+J_i)$ versus V_p

would yield a straight line. The slope of this line would give T_e. Experimentally, it is found that this plot is not always linear and it is therefore of interest to determine $g(v_z)$ in terms of the probe curve. This can be done quite simply. Taking the derivative of 2.46 with respect to V_p we obtain

$$\frac{\partial J_p}{\partial V_p} = -\frac{e^2}{m} g\left(\sqrt{2\frac{e}{m}V_p}\right)$$

or

$$g(v_z) = -\frac{m}{e^2}\frac{\partial J_p}{\partial V_p}; \quad v_z = \sqrt{2\frac{e}{m}V_p} \tag{2.48}$$

Thus we see that for a planar probe the distribution of velocities normal to the probe surface can be determined from the first derivative of the probe current with respect to the probe voltage. We are assuming, of course, that the probe current is equal to the area of the probe times the current density and that the probe area is constant. For a planar probe the area is constant, while for finite geometries the area is generally a function of V_p.

The above analysis will be used to interpret the data presented in this thesis.

To point out the differences between this theory and that developed by Druyvesteyn (10) which is usually used, we will present the Druyvesteyn analysis for the same case of a planar probe. The only difference is that Druyvesteyn did the analysis assuming an isotropic

---

(10) M. J. Druyvesteyn, Z. Physik 64, 781 (1930).

speed distribution $f(v)$ rather than the directed distribution $g(v_z)$. To carry out this analysis it is necessary to obtain $dn(v_x)$ in terms of $f(v)$ instead of $g(v_z)$. This can be done by noting that electrons arriving at the probe with the same speed v and angle θ with respect to a normal to the probe surface have the same v_z (i.e., $v_z = v \cos \theta$). Thus we have

$$dn(v_z) = dn(\theta)\, dn(v) \tag{2.49}$$

where $dn(\theta)$ is the percent of the electrons arriving at the probe at an angle θ with respect to the probe normal, and $dn(v)$ is the density of electrons with speeds in the range v to $v+dv$. For an isotropic distribution $dn(\theta)$ is the ratio of the differential solid angle $d\Omega$ at θ to the total solid angle 4π. The quantity $dn(v)$ is $4\pi v^2 f(v)\, dv$ from our previous definition of $f(v)$. Here again we have assumed an isotropic distribution. Thus,

$$dn(v_z) = \frac{2\pi \sin\theta\, d\theta}{4\pi}\, 4\pi v^2 f(v)\, dv \tag{2.50}$$

and the electron current density to the probe is

$$J_e = \underset{\substack{\text{all possible} \\ v \text{ and } \theta}}{\int\int} e v_z\, 2\pi \sin\theta\, d\theta\, v^2 f(v)\, dv \tag{2.51}$$

Again the limits are determined by energy considerations. That is,

$$\frac{1}{2} m(v \cos\theta)^2 \geq eV_p \tag{2.52}$$

Therefore we have

$$J_e = \int_{\sqrt{2\frac{e}{m}V_p}}^{\infty} dv \int_0^{\cos^{-1}\sqrt{\frac{2eV_p}{mv^2}}} d\theta \; ev^3 \cos\theta \, 2\pi \sin\theta f(v)$$

or

$$J_e = \frac{e}{4} \int_{\sqrt{2\frac{e}{m}V_p}}^{\infty} \left\{1 - \frac{2eV_p}{mv^2}\right\} vf(v)\, dv \tag{2.53}$$

Differentiating this expression twice with respect to V_p we obtain

$$f(v) = \frac{m^2}{2\pi e^3} \frac{\partial^2 J_p}{\partial V_p^2} \tag{2.54}$$

where v is the velocity corresponding to V_p (i.e., $v = \sqrt{2\frac{e}{m}V_p}$). This $f(v)$ is not the distribution function that is usually meant when speed distributions are being discussed. The usual one, $f'(v)$, is the function such that $f'(v)\,dv$ gives the density of electrons with speeds between v and $v+dv$. From the discussion leading to equation 2.50 we see that

$$f'(v) = 4\pi v^2 f(v) \tag{2.55}$$

Thus in terms of the probe curve we have

$$f'(v) = \frac{4mV_p}{e^2} \frac{\partial^2 J_p}{\partial V_p^2} \tag{2.56}$$

Since all measurements cited in the literature give $f'(v)$ or the energy distribution function, we will compare the above result for $f'(v)$ with that found earlier for $g(v_z)$ in equation 2.48.

First we note that the Druyvesteyn analysis requires the second derivative of the probe curve while the $g(v_z)$ equation involves only the first derivative. It is therefore much easier to implement the $g(v_z)$ theory experimentally.

Second, the expression for $f'(v)$ contains V_p explicitly along with $\frac{d^2I_p}{dV_p^2}$. Thus to obtain the correct functional form for $f'(v)$ it is necessary to determine V_p accurately. Since V_p does not appear in the expression for $g(v_z)$ the incorrect determination of V_p will merely shift the $g(v_z)$ curve in velocity but will not alter its shape. This point is of interest because it is not in general easy to determine experimentally the plasma potential, and therefore V_p. Mott-Smith and Langmuir (11) have shown that for a Maxwellian distribution the probe curves for planar, cylindrical and spherical geometries all have an inflection point at $V_p = 0$. Therefore in the work described here this inflection point is taken to be $V_p = 0$ on the plasma potential. More recent work by Wehner and Medicus (12,13) and Waymouth (14) has shown that this may be in error due to the variation of the work function

---

(11) H. M. Mott-Smith, I. Langmuir, Phys. Rev. 28, 727 (1926).
(12) G. Wehner, G. Medicus, J. Appl. Phys. 23, 1035 (1952).
(13) G. Medicus, Proc. of 5th Internation Conference on Ionization Phenomena in Gases, Vol.II, Ed., H. Maecker (North Holland Publishing Co., Amsterdam 1962), p. 1397.
(14) J. F. Waymouth, MIT Research Laboratory of Electronics Technical Report 406 (1962).

over the probe surface and the perturbing of the plasma by the probe.

A third point of comparison is that the Druyvesteyn analysis assumes an isotropic distribution function. If the distribution is anisotropic the analysis is not valid. On the other hand, no such assumption was necessary in the analysis using $g(v_z)$. In fact the anisotropy of the distribution can be measured by changing the plane of the probe.

The above derivations were carried out under the assumption of a planar probe. However, Druyvesteyn showed equation 2.54 to be valid for cylindrical and small spherical probe geometries as well. The only assumption was that the distributions were isotropic.

We will now show that equation 2.48 giving $g(v_z)$ is also valid for cylindrical and small spherical geometries. We know that $f(v)$ and $g(v_z)$ are related as follows

$$g(v_z) = \int_{-\infty}^{\infty}\int f(v)\, dv_x dv_y \tag{2.57}$$

Writing this in terms of a set of polar coordinates $r^2 = v_x^2 + v_y^2$, $\theta = \tan^{-1}\frac{v_y}{v_x}$ gives:

$$g(v_z) = \int_0^{2\pi} d\theta \int_0^{\infty} r\,dr\, f(v) \tag{2.58}$$

which for an isotropic distribution becomes

$$g(v_z) = 2\pi \int_0^{\infty} f(v)\, r\,dr = 2\pi \int_0^{\infty} f\left(\sqrt{r^2 + v_z^2}\right) r\,dr \tag{2.59}$$

Setting $u^2 = r^2 + v_z^2$ we obtain:

$$g(v_z) = 2\pi \int_{v_z}^{\infty} f(u)\, u\, du \tag{2.60}$$

Taking the derivative of this equation with respect to v_z gives

$$\frac{\partial g(v_z)}{\partial v_z} = 2\pi \frac{\partial}{\partial v_z} \int_{v_z}^{\infty} v f(v)\, dv = -2\pi\, v_z f(v_z)$$

so

$$f(v) = -\frac{1}{2\pi\, v_z} \left.\frac{\partial g}{\partial v_z}\right|_{v_z = v} \tag{2.61}$$

Combining this equation with 2.54 we obtain

$$\left| \frac{-1}{2\pi\, v_z} \frac{\partial g}{\partial v_z} \right|_{v_z = v} = \frac{m^2}{2\pi e^3} \frac{\partial^2 J_p}{\partial V_p^2} \tag{2.62}$$

or

$$-\frac{1}{v} \frac{\partial g(v)}{\partial v} = \frac{m^2}{e^3} \frac{\partial^2 J_p}{\partial V_p^2}$$

but $v = \sqrt{2 \frac{e}{m} V_p}$ so we can write this as

$$-\frac{\partial g}{\partial V_p} = \frac{m}{e^2} \frac{\partial^2 J_p}{\partial V_p^2} \tag{2.63}$$

which, when integrated once, yields

$$g = -\frac{m}{e^2} \frac{\partial J_p}{\partial V_p} + \text{constant} \tag{2.64}$$

The constant must be zero because the integral of $g(v_z)$ over all v_z must give n and any non-zero constant in g would produce an

infinite value for this integral. This expression (which is identical to that found for $g(v_z)$ in our planar probe theory) was derived assuming only that the distribution is isotropic and that Druyvesteyn's analysis is correct. Since Druyvesteyn's analysis is only correct for isotropic distributions, the above expression for $g(v_z)$ is valid whenever Druyvesteyn's second derivative theory is valid. This is quite interesting because it means that for isotropic distributions the expression $g(v_z) = -\frac{m}{e^2}\frac{\partial J_p}{\partial V_p}$ is valid for planar, cylindrical and small spherical probe geometries.

We see then that if we are dealing with isotropic distributions either theory can be applied depending on whether $f(v)$ or $g(v_z)$ is wanted. However, in the more common case of anisotropic distributions the $f(v)$ theory is incorrect and we are forced to resort to a planar probe and the theory for the directed distribution $g(v_z)$.

2.4 Analysis of Planar Guard-Ring Probe

In the preceding discussion a planar probe has meant an infinite plane conductor. In practice this never exists but we can approximate it by using a finite planar probe with a guard ring. Such a probe is shown in Figure 2.4. The probe collecting surface is divided into a small center section and the guard ring which completely surrounds this section. In using such a probe both sections are set at the same potential but only the current to the center section is measured. Thus we find the volt ampere characteristic of only the center section. The guard ring serves merely to remove the effects of the edges from our probe curve; that is, we assume that any effect due to the finite probe

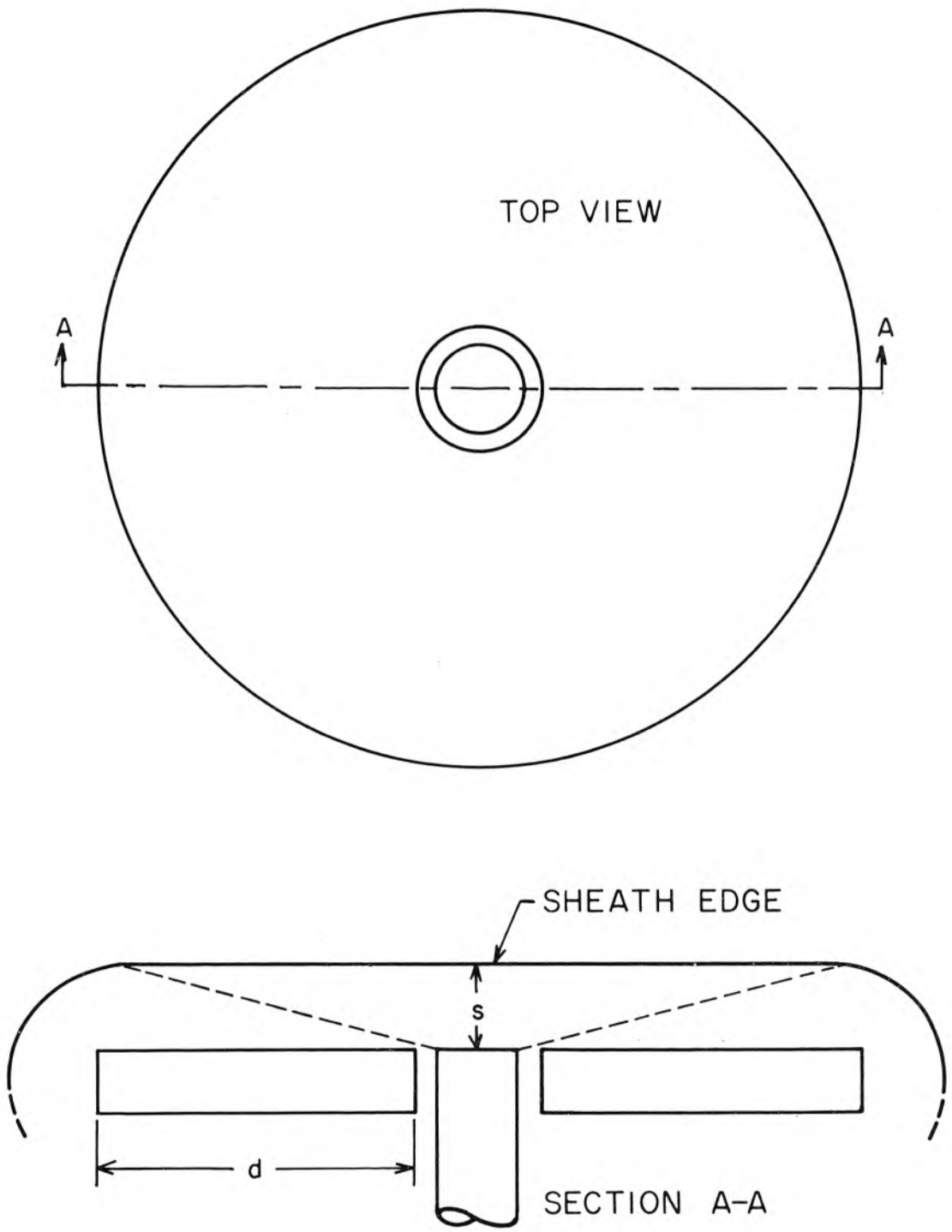

Fig. 2.4 Planar Guard Ring Probe

size influences only the current to the guard ring and not the center section.

To determine the validity of this assumption we must discuss one other aspect of plasma diagnostics using probes. This is the fact that the potential on the probe produces a field which penetrates into the plasma. In Figure 2.4 the distance the field penetrates from the probe is denoted by s and will hereafter be called the sheath thickness. This sheath thickness is not well defined--in fact, it can be shown that the field penetrates an infinite distance. However, for sufficiently high electron density and high enough probe potentials the sheath is a meaningful concept (15). For these conditions the sheath region is the same as a space charge limited diode. That is, there exists a sheath of positive space charge around the probe and, at the outside of the sheath, the potential and the field are zero. For these conditions, in a planar geometry, we can write the following expression relating ion current density to the probe, probe potential, and sheath thickness:

$$|J_i| = 2.335 \times 10^{-6} \sqrt{\frac{m}{M}}\, V_p^{3/2}\, s^{-2} \tag{2.65}$$

or

$$s = 1.53 \times 10^{-3} |J_i|^{-1/2}\, V_p^{3/4} \left(\frac{m}{M}\right)^{1/4}$$

but for a Maxwellian distribution for the ions and negative probe potentials, equation 2.47 gives $|J_i| = eN_i \sqrt{\frac{kT_i}{2\pi M}}$. Therefore

---

(15) S. Self, Phys. Fluids 6, 1762 (1963).

$$s = 1.53 \times 10^{-3} e^{-1/2} \left(\frac{2\pi m}{kT_i}\right)^{1/4} V_p^{3/4} N_i^{-1/2} \tag{2.66}$$

Let us now calculate the probe current due to electrons which are collected by the center section of the probe and pass through the planar portion of the sheath; that is, the electrons which pass through the cone shown dotted in Figure 2.4. The ratio of this current to the current collected by the same area of an infinite planar probe is a reasonable criterion as to the effectiveness of the guard ring probe.

We can find the number of electrons passing through the cone by noting that these are defined by having a transit time across the sheath (t_s) which is less than the time it takes them to move a distance d tangential to the probe. Calling the latter t_d we can write

$$t_s \leq t_d = \frac{d}{\sqrt{v_x^2 + v_y^2}} \tag{2.67}$$

but $$t_s = -\int_{z=s}^{0} \frac{dz}{v_z}$$

where $$v_z = \sqrt{v_z^2(s) - 2\frac{e}{m} V(z)} \tag{2.68}$$

If the potential in the sheath $V(z)$ varies as the p^{th} power of z we can write

$$t_s = \int_s^0 \frac{-\,dz}{\sqrt{v_z^2(s) - 2\frac{e}{m} V_p \left(1 - \frac{z}{s}\right)^P}} \tag{2.69}$$

We are interested in the greatest value of t_s and this occurs for the electron which reaches the probe with zero velocity. For this electron $v_z^2(s) = 2\frac{e}{m} V_p$ so we have

$$t_{s_{max}} = \int_s^0 \frac{-\,dz}{\sqrt{2\frac{e}{m}V_p}\sqrt{1 - \left(1 - \frac{z}{s}\right)^P}} = \frac{1}{\sqrt{2\frac{e}{m}V_p}} \int_0^s \frac{s^{P/2}\,du}{\sqrt{s^P - u^P}} \tag{2.70}$$

We can evaluate this for $p = 1$ and $p = 2$ obtaining

$$t_{s_{max}}(p=1) = 2s\sqrt{\frac{m}{2e\,V_p}}$$

$$t_{s_{max}}(p=2) = s \sin^{-1}\frac{u}{s}\Bigg|_0^s \sqrt{\frac{m}{2eV_p}} = \frac{\pi}{2} s \sqrt{\frac{m}{2eV_p}} \tag{2.71}$$

If the potential in the sheath follows the space charge limited diode condition $(V(z) \propto z^{4/3})$, $t_{s_{max}}$ will lie between the two values found above. Taking the worst condition (largest $t_{s_{max}}$) our inequality becomes

$$2s\sqrt{\frac{m}{2e\,V_p}} \leq \frac{d}{\sqrt{v_x^2 + v_y^2}} = \frac{d}{r} \tag{2.72}$$

or $$r \leq \frac{d}{2s}\sqrt{2\frac{e}{m}V_p} \quad .$$

The current due to electrons which meet this criterion is

$$eA \int_{\sqrt{2\frac{e}{m}V_p}}^{\infty} v_z dv_z \iint_{v_x^2+v_y^2=0}^{(\frac{d}{2s})^2 \frac{2eV_p}{m}} dv_x dv_y f(v_x, v_y, v_z) \tag{2.73}$$

whereas the current to the same area of an infinite probe is

$$eA \int_{\sqrt{2\frac{e}{m}V_p}}^{\infty} v_z dv_z \iint_{v_x^2+v_y^2=0}^{\infty} dv_x dv_y f(v_x, v_y, v_z) \tag{2.74}$$

If we assume a Maxwellian distribution function the ratio of these two currents is

$$\frac{\frac{d}{2s}\sqrt{\frac{2eV_p}{m}} \int_{r=0} e^{-\frac{mr^2}{2kT_e}} rdr}{\int_{r=0}^{\infty} e^{-\frac{mr^2}{2kT_e}} rdr} = (\frac{d}{2s})^2 \frac{eV_p}{kT_e} \int_0 e^{-u} du \tag{2.75}$$

Thus the ratio is

$$1 - e^{-(\frac{d}{2s})^2 \frac{eV_p}{kT_e}} \tag{2.76}$$

and if we substitute equation 2.66 for s we obtain

$$1 - e^{-\frac{e^2 d^2 N_i}{9.34 \times 10^{-6} T_e} \sqrt{\frac{T_i}{2\pi m k V_p}}}$$

or

$$1 - e^{-3.09 \times 10^{-7} \frac{N_i d^2}{T_e} \sqrt{\frac{T_i}{V_p}}} \qquad (2.77)$$

We would like this ratio to approach 1 . For small V_p this is the case because the sheath thickness is very small. However, as stated before, the space charge limited equation is not valid for small V_p . In fact, it takes V_p of the order of at least $\frac{kT_e}{e}$ to form a stable sheath (16). This planar criterion is therefore suspect for voltages less than $\frac{kT_e}{e}$.

Even though the approximations used here (Maxwellian distribution, space charge limited diode sheath) are not applicable in all cases, equation 2.77 shows what parameters control the usefulness of a guard ring probe. It is basically a statement that the sheath thickness should be small compared to the guard ring width. The required ratio of these dimensions depends on the number of high energy electrons, here specified in terms of T_e . We will return to this expression when discussing the experimental results in order to determine whether or not the guard ring probe used can be assumed planar.

---

(16) D. Bohm, Characteristics of Electrical Discharges in Magnetic Fields, Ed., A. Guthrie, R.K. Wakerling (McGraw-Hill Book Company Inc., New York, 1949) p. 77.

III. EXPERIMENTAL TECHNIQUE

3.1 Description of Discharge Tubes and Vacuum System

The experiments to be described in the remaining sections of this thesis were performed in hot cathode rare gas discharges. A schematic drawing of the type of tubes used is shown in Figure 3.1. The tubes had a pyrex glass envelope 50 mm in diameter and 80 cm long. Ports with o-ring gland seals were provided at two points along the length of the tube so that probes could be inserted. This type of port allowed the probe to be moved radially within the tube and also to be rotated about its axis. The hot cathode consisted of a coiled tungsten wire which was directly heated by passing approximately 25 amperes of d-c or a-c current through it. Most of the data were taken using d-c heater power, but it was found that the probe curves were not altered when a-c was used. The tube anodes were shallow stainless steel cups. A valve was provided at the gas inlet to the tube so that it could be filled and then valved off.

These tubes were placed on a vacuum system consisting of mechanical fore pump, oil diffusion pump, and absorption trap filled with activated alumina. This system was capable of pumping the tubes down to a pressure of 10^{-7} mmHg. While on the vacuum system, all parts of the tube which could be baked were heated to 300°C using a heating tape. The o-ring seals in the ports made it impossible to bake this portion of the tubes. However, this was not felt to be important, as the discharge did not enter this unbaked portion. The tubes were then filled with whatever gas was to be used (neon or

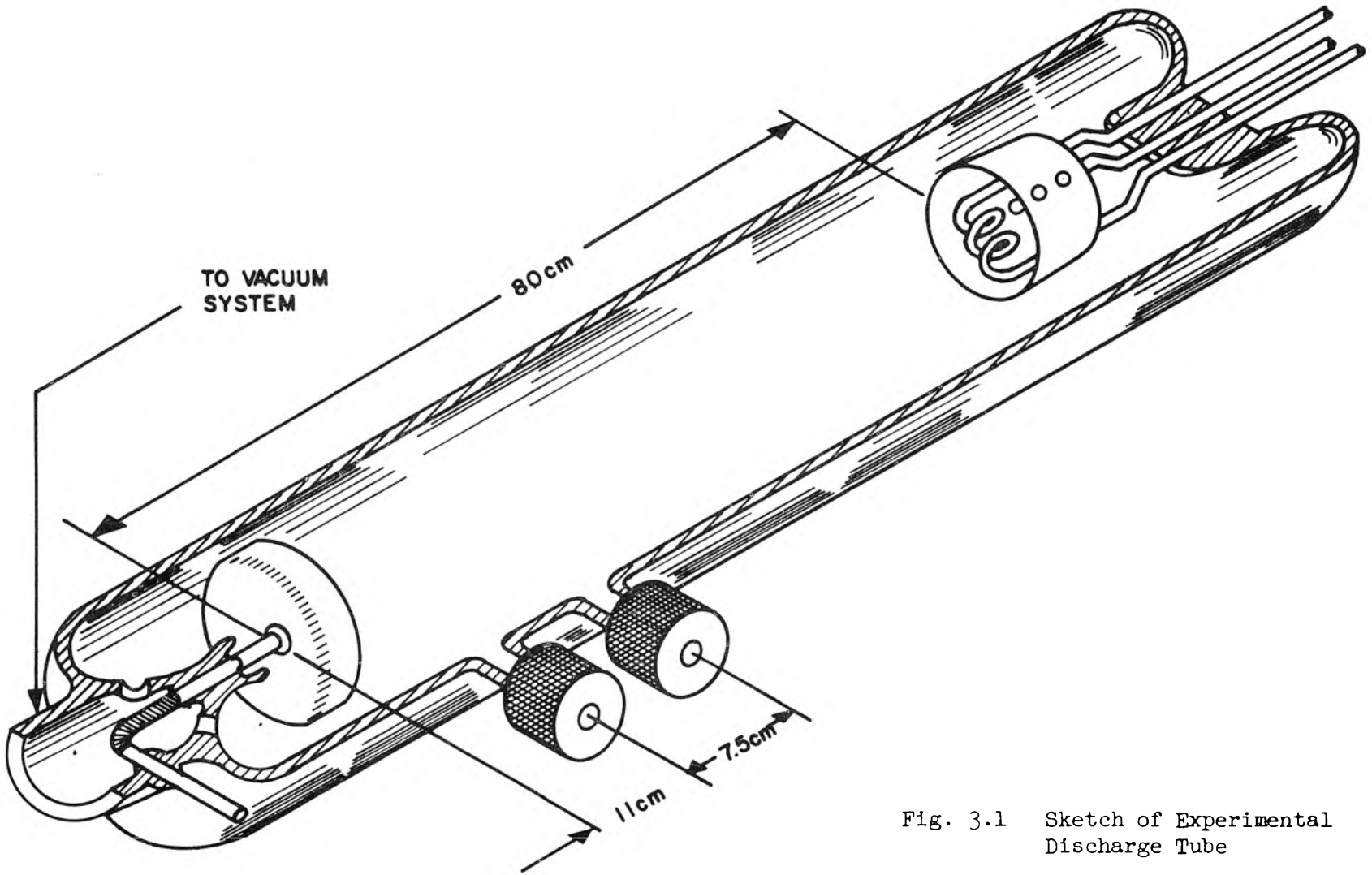

Fig. 3.1 Sketch of Experimental Discharge Tube

helium) and the discharge was run at or above the highest current used experimentally for approximately one-half hour. This procedure was repeated several times (usually six to eight). In this way the discharge was used to clean the tubes further and the contaminants were pumped and purged from the system. The success of this system for processing the tubes is demonstrated in the fact that data taken several months apart under the same conditions yielded results which agreed within ten percent.

3.2 Description of Probe

The probe used to measure the directed distribution functions consisted of three orthogonal planar guard ring probes as shown in Figure 3.2. This probe was placed on the end of a 0.092-inch stainless steel tube. Four wires were run from the probe through the tube to the instrumentation provided for analysis. The ends of three of the wires were the three active probe surfaces, while the fourth wire was attached to the guard ring. The wires were 0.01 inches in diameter so they provided a probe area of 5.07×10^{-8} m^2. Molybdenum was used for the wires and the guard ring. The four wires were insulated from each other and the tube by passing them through four-hole ceramic tubing which ran the full length of this stainless steel tube. The wires were then positioned in the 0.015-inch holes of the guard ring, and the guard ring attached to the end of the tube using bonding agent number R313 manufactured by the Carl H. Biggs Company. In the resulting composite probe the d-c resistances between probes, probes and guard-ring, probes and tube, and guard-ring and tube, were all of the order

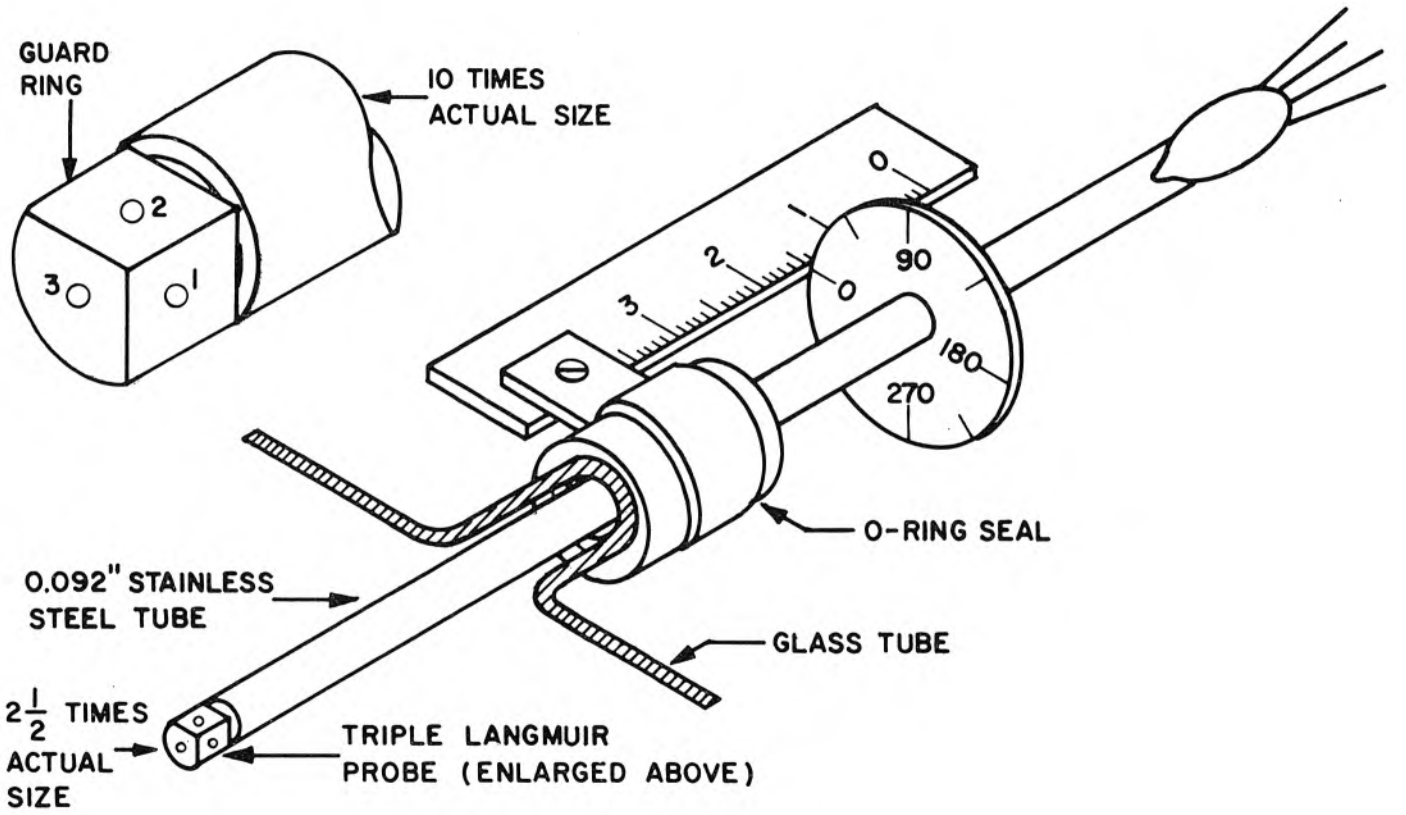

Fig. 3.2 Sketch of Triple Guard Ring Probe

10^9-10^{10} ohms. As much as possible the bonding agent was kept out of the space between probes and guard rings. This was done so that hydrocarbons from this material would not contaminate the discharge due to bombardment by energetic particles in the discharge. Finally the probe surfaces were hand lapped and polished. The probe was then immediately placed in a vacuum to reduce the possibility of surface contamination. In order to determine whether the probe surfaces were clean, two of the probe surfaces (with the same orientation) were used to obtain volt-ampere curves at the same point in the discharge. The probes were considered clean and the rest of the apparatus assumed to be operating properly, if these two curves agreed within a few percent. This was found to be a highly useful technique in that it brought to light many times, probe contamination and instrumentation problems which might otherwise have been overlooked.

3.3 Instrumentation

A block diagram of the experimental setup is shown in Figure 3.3. The three probes and the guard ring were all swept with a one-tenth of cycle per second triangular voltage waveform. This allowed the derivative of the probe curve to be obtained by taking a time derivative of the probe current because time and voltage were linearly dependent. A switching arrangement was provided so any one of the probe currents or the guard ring current could be measured. The sensing resistors for the probes were 30 kΩ , while that for the guard ring was 100Ω . This was so the difference in currents to the probes and guard ring (due to their different areas) would not cause the two to be at different potentials. The stainless steel tube was usually

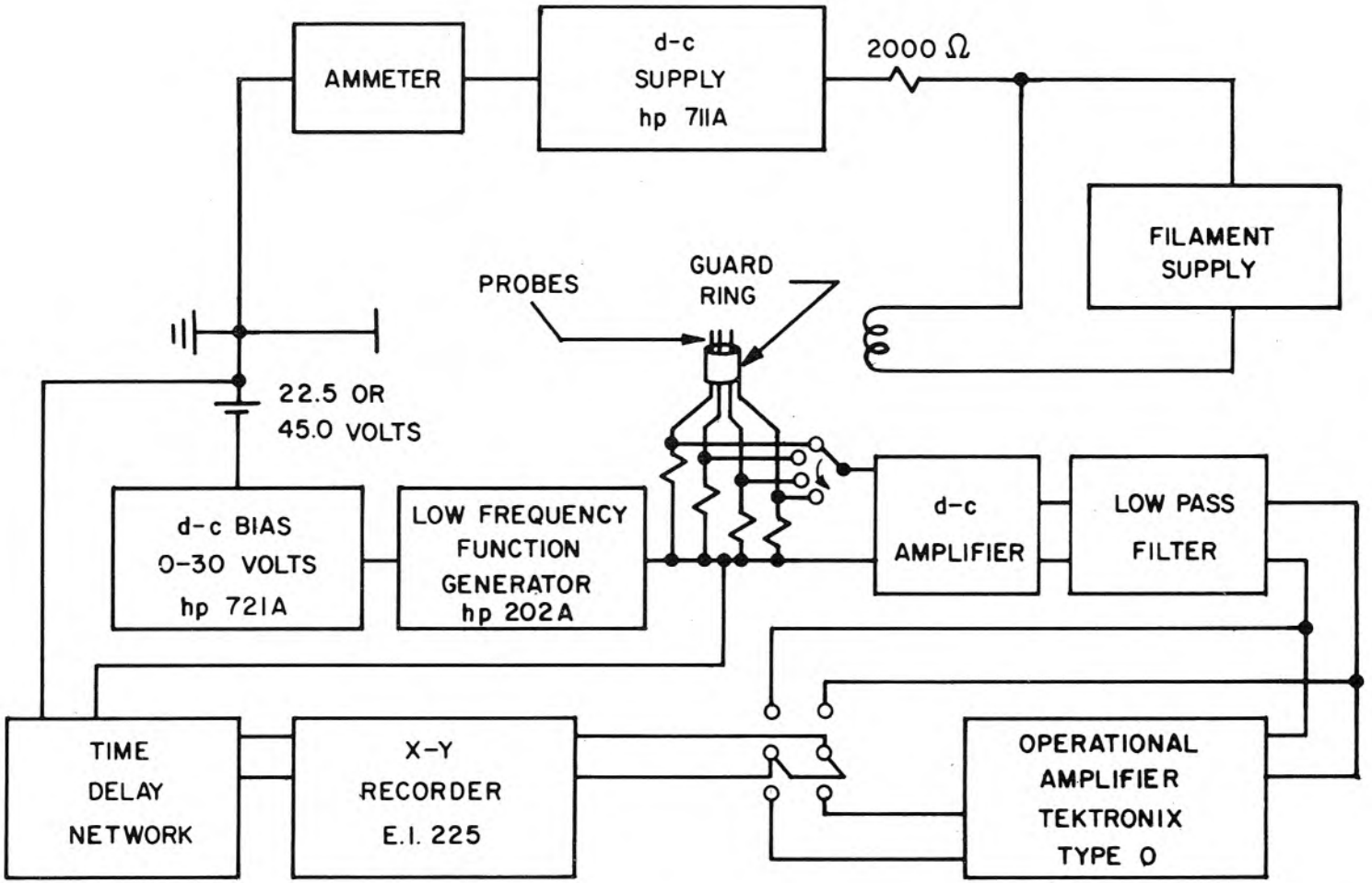

Fig. 3.3 Block Diagram of Experimental Apparatus

left floating so that it drew no current. The effect of this tube on the probe curves was checked by biasing it at various potentials with respect to the plasma (5 to 40 volts negative) and then taking a set of probe curves. Over this range of potentials the effect on the probe curves was negligible.

The voltage developed across the sensing resistors was fed to a d-c amplifier with a gain of 30. From here the signal passed through a low pass filter and then either directly to the y-axis of an x-y recorder, or to a Tektronix type O operational amplifier where it was differentiated and then applied to the x-y recorder. The x-axis of the recorder was driven by the triangular voltage which was used to sweep the probes delayed by 28.6 milliseconds. This delay was to compensate for a similar delay in the y-axis due to the low pass filter. We see than that with this system it was possible to plot either the probe curve or the derivative of the probe curve directly on an x-y recorder.

The filter was necessary only to rid the signal of noise due to 60 cycle pickup in the leads and noise from the d-c amplifier; that is, the noise level due to the discharge was no greater than the system noise. Data were taken only in current-pressure regions of the discharge where no oscillations could be detected optically with a silicon solar cell, or seen as voltage fluctuations across the discharge tube, or discerned when viewing the derivative of the probe curves on a 30 megacycle oscilloscope. In the operating regions of the discharge where data were taken there was no discernable change in the noise seen on the derivative of the probe curve when the discharge was turned on and off.

The obvious question is, why the filter? The answer is that for plotting probe curves only (volt-ampere characteristics) it was unnecessary, but the differentiator enhanced the high frequency noise to a point that even with no input to the d-c amplifier the x-y recorder was unstable.

The filter consisted of two RC "twin-tee" networks and an RC low pass filter in cascade. The two "twin-tees" had transmission zeros at 60 cycles and 400 cycles, giving a transmission curve for the filter as shown in Figure 3.4. Also shown on the figure is the circuit diagram.

3.4 Data Taking Procedure

Data were taken in neon and helium discharges in the range of pressures from 0.4 to 1 mmHg. The discharge current was adjusted so that the discharge was quiescent as described in the previous section. This quiescent region was obtained for currents in the range of 50 to 100 milliamperes.

In the following discussion the three orthogonal probes will be designated by number as shown on Figure 3.2. The probes lying in planes parallel to the axis of the probe support tube are numbered one and two and the probe lying in a plane normal to the probe axis is number three.

When it had been ascertained that the probes were clean and the instrumentation was operating correctly, the tube was filled with gas at the desired pressure (this pressure was measured using a Piranni gauge). Next the current was set and data taken in the following

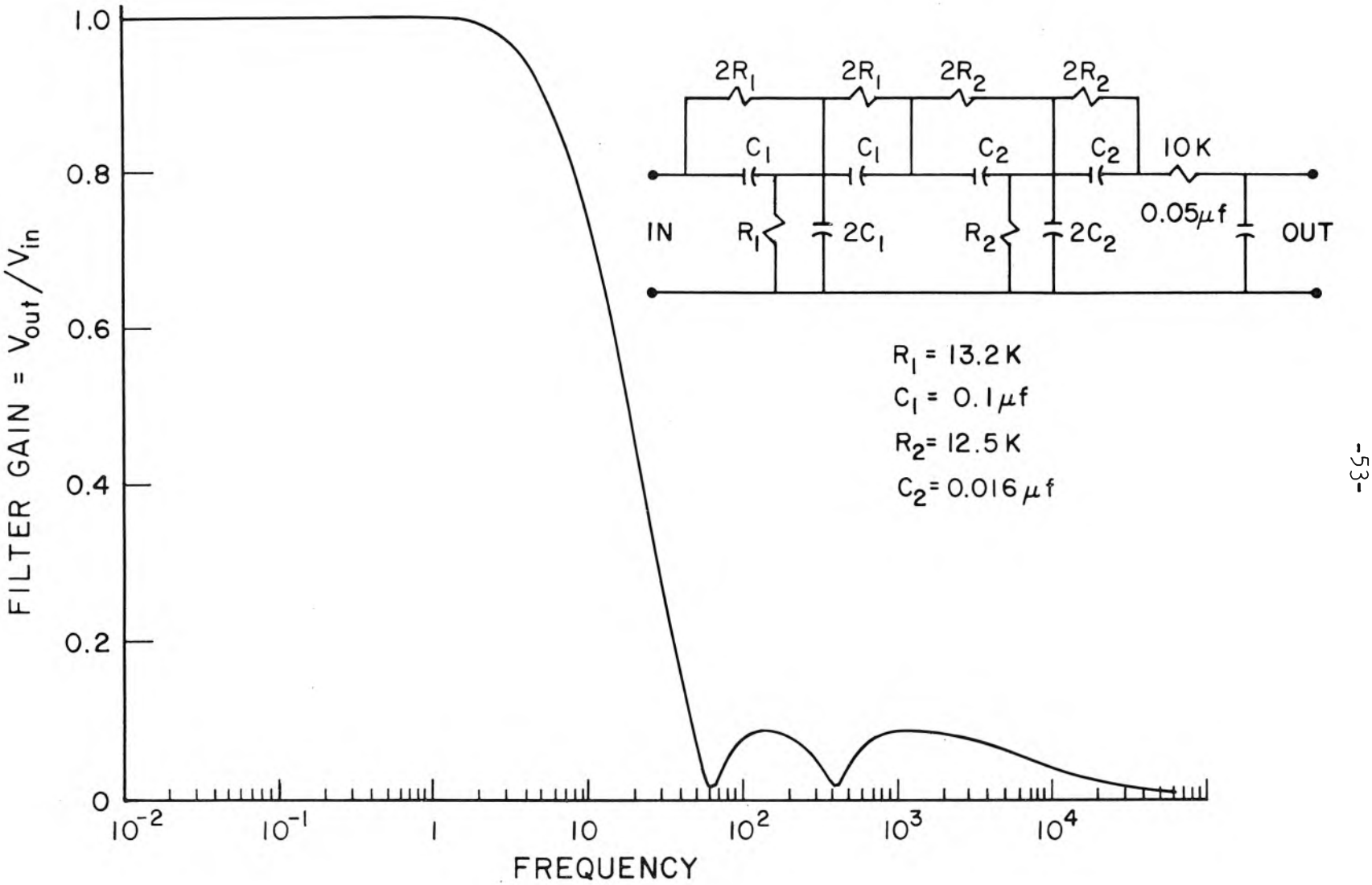

Fig. 3.4 Low Pass Filter Transmission Characteristic and Circuit Diagram

sequence. The probes were set so that one and two were 0.5 cm from the tube wall. Then probe curves were obtained for probe one facing the cathode, the anode, and in an azimuthal direction in the discharge tube. The same three curves were then taken with probe number two. This was done to insure that the results were never a function of which probe was used. Next, two curves were obtained using probe number three. The difference between these curves was that the probe was rotated by ninety degrees. Again rotating the probe by ninety degrees between measurements, two curves were obtained for the guard ring. This led to a set of ten curves as shown in Figure 3.5. The same ten measurements were then made again, only this time the derivative was plotted versus probe potential (Figure 3.6). Next the probe was set so that probes one and two were 1.0 cm, 1.5 cm, and 2.0 cm from the tube wall. At each position the same ten probe curves and ten derivative curves were obtained. This same procedure was carried out for at least three different gas pressures and three different tube currents for each pressure. The probe was then moved to the other tube port and the same set of curves obtained. This led to a set of curves which coarsely covered variation of the following parameters:

1. Gas pressure
2. Tube current
3. Orientation of probe surface
4. Radial position of probe within tube
5. Longitudinal position of probe

As stated previously, these data were obtained for neon and helium discharges. Argon was tried but it was found that no quiescent discharge existed within the obtainable range of discharge conditions.

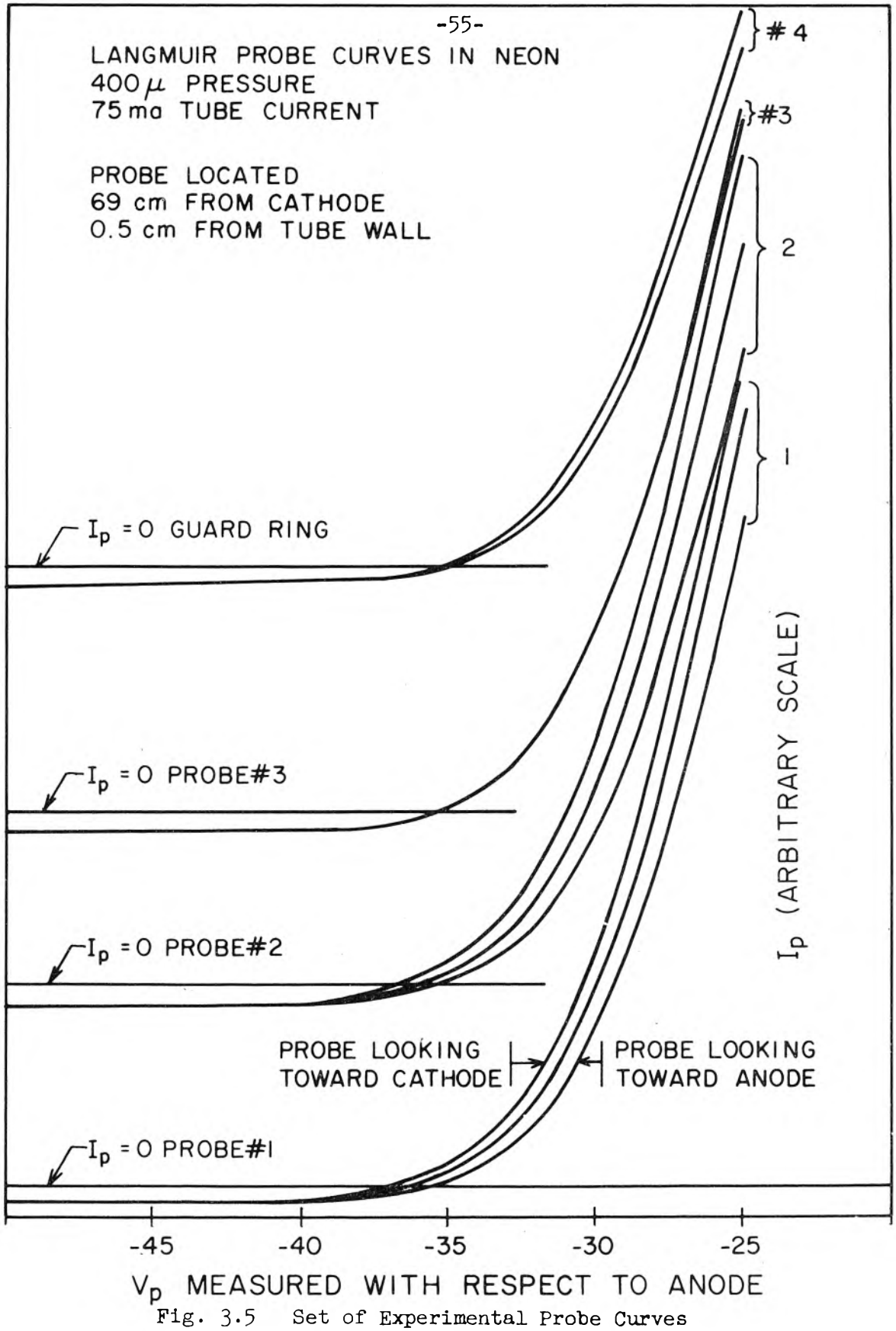

Fig. 3.5 Set of Experimental Probe Curves

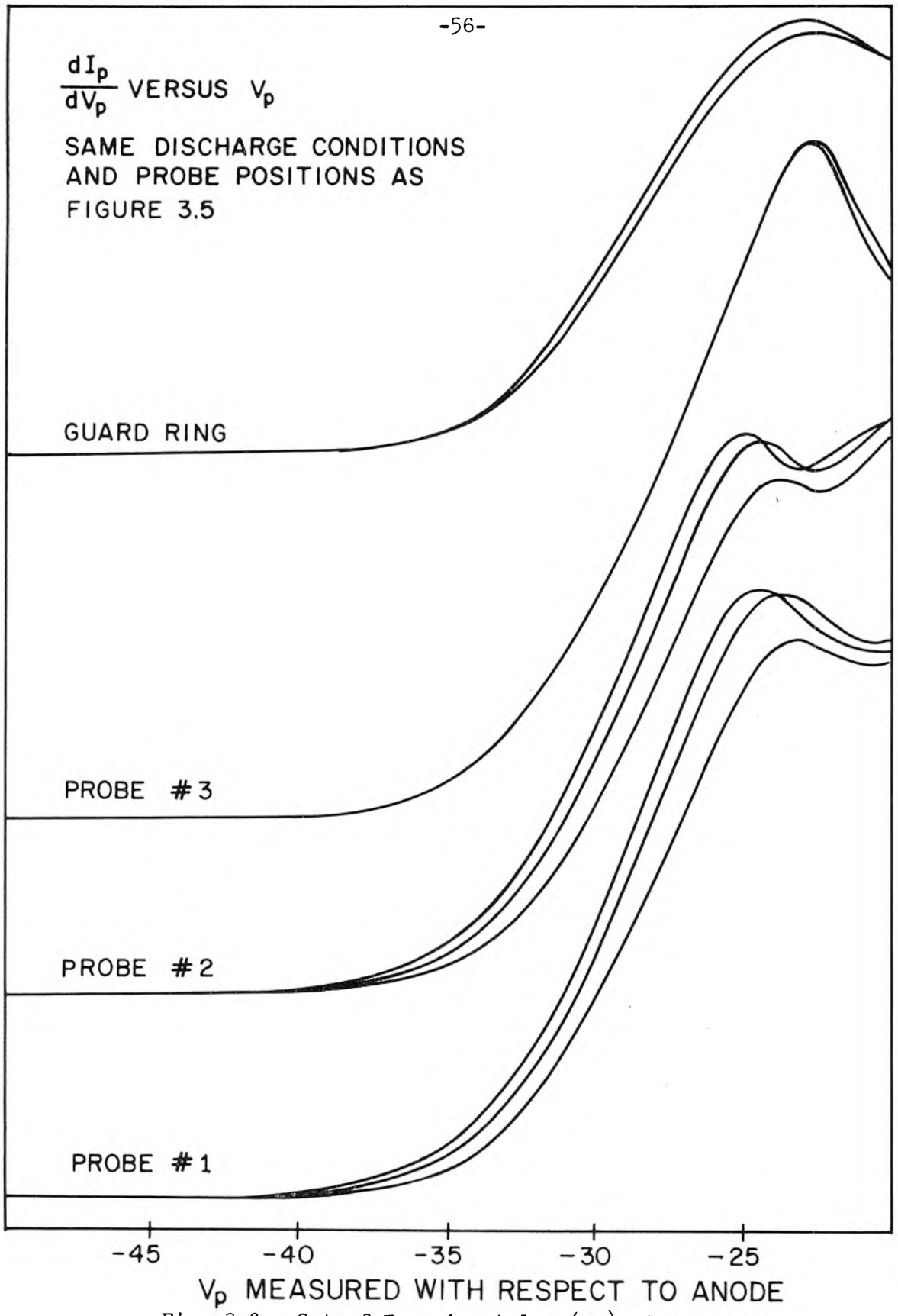

Fig. 3.6 Set of Experimental $g(v_z)$ Curves

IV. EXPERIMENTAL RESULTS

4.1 Data Reduction

Preliminary data reduction consisted of perusal of the wealth of curves to determine general features and any noticeable peculiarities. Then semi-log plots of approximately one-fourth of the probe curves were made to ascertain whether or not the distributions were Maxwellian. At this time groups of $g(v_z)$ curves (derivative curves) which were found to be typical were replotted versus v_z instead of V_p so that they could be compared with the theory presented in Section 2.2. For these curves the $V_p = 0$ point was taken as the point where the probe curves had an inflection point or the derivative curves a maximum. However, this inflection point would be at $V_p = 0$ only for a distribution with no drift velocity normal to the probe. For this reason the $V_p = 0$ point was determined from probes one and two when they were looking in an azimuthal direction. As the probe surface did not contain the center line of the probe supporting tube, rotating the probe about its axis also moved it longitudinally along the discharge tube. Since there exists a field along the tube, the $V_p = 0$ point for the azimuthally looking probe is not the same as for the same probe when it is pointed toward the anode or the cathode. This was taken into account by determining the axial field from corresponding probe curves taken at the two tube ports. Knowing this field and the probe geometry it was possible to calculate the change in V_p due to probe rotation.

The electron density was then obtained by graphically integrating the curves $g(v_z)$ with a polar planimeter. This number was compared with the one found by using the ion saturation current. The $g(v_z)$

curves for velocities parallel to the tube axis were then multiplied by v_z and the resulting curves integrated in order to calculate the tube current from the measured distribution functions. This number was compared with the measured tube current.

Beyond this, the experimental curves were compared with those derived in the theory section (and others) to see if they could be simply described analytically. Calculations were made to determine whether the low ionization, high field assumptions of the theory section were valid. Also checked was the planar probe criterion as discussed in Section 2.4.

4.2 General Properties of Measured Distributions

Let us look first at the general properties of the measured distribution functions. Most significantly, none are Maxwellian. This is shown by the nonlinearity of the semi-logarithmic plots and by curve fitting on the $g(v_z)$ curves plotted versus v_z. Sufficiently far from the cathode the distributions are found to be nearly Druyvesteyn. The deviations from Druyvesteyn can be explained in terms of the high longitudinal field which produces an anisotropy and the fact that the mean free paths for neon and helium are energy dependent.

The effect of the dependence of the mean free path on energy is qualitatively simple. If the mean free path increases with energy (helium) the high energy electrons will gain more energy per mean free path than the low energy ones. This tends to increase the number of high energy electrons above that found for a constant mean free path.

The opposite case where the mean free path decreases with energy (neon) has the effect of concentrating the electrons about the mean energy. That is, there are fewer high and low energy electrons than are found for the constant λ case. Both of these effects are observed in the measured distribution functions. The above qualitative argument has been shown to be valid theoretically by Allen (1). This was done by numerically solving equation 2.22 for the correct dependence of λ on energy.

The anisotropy produced by the field is usually discussed in terms of a drift velocity. The measured distributions show that it would be more accurate to say that the distributions are shifted in energy. The magnitude of the energy shift is nearly the mean free path of the electrons times the longitudinal field. This is seen by shifting all points on the distribution functions by an amount of the order of the longitudinal field times the mean free path for the energy class being considered and noting that the resulting curves are symmetrical about zero velocity. This was done for approximately one-fourth of the data and in all cases the resulting curves were very nearly symmetric. Because the product of the mean free path times the field gives only an order of magnitude value for the energy shift, the needed energy shift was determined by noting how far the peak of the measured functions was shifted from zero. This gave a value for the zero energy shift and the shift necessary for any other energy class

---

(1) Harriet W. Allen, Phys. Rev. 52, 707 (1937).

of particles was found by using this number and the ratio of the low energy mean free path to the mean free path at the energy in question. As far as the author can determine, this is the first time it has been shown that a strong field shifts the electron distribution in energy rather than merely imparting a drift velocity (i.e., a velocity shift).

Before presenting specific curves showing the above properties it is in order to give some experimental support for their validity. The one measured discharge parameter that can be calculated directly from the measured distribution functions is tube current. The value of tube current density flowing at a particular point is given by

$$J_{tube} = e \int_{-\infty}^{\infty} v_z g(v_z)\, dv_z \qquad (4.1)$$

This integration was carried out graphically at points located 0.5, 1.0, 1.5 and 2.0 cm from the wall of the tube. The radial current distribution was then plotted and the average current density found. This number was then multiplied by the cross-sectional area of the tube and the results compared with the measured tube current. The results of these calculations are shown in Table 4.1.

This table brings out the possibility of a systematic error in the data in that all the values obtained by integrating $g(v_z)$ are low. It is felt that this is due to the rather large size of the total probe consisting of three planar probes. At low probe potentials the probe draws currents of the order of one to two milliamperes. This much current may tend to decrease the electron concentration and

TABLE 4.1

Comparison of Measured and Calculated Tube Currents

Discharge Description	Neon P = 400μ				Helium P = 1000μ		Helium P = 500μ	
Distance from probe to cathode (cm)	69	61.5	69	61.5	69	61.5	69	61.5
Measured tube current (ma)	100	100	75	75	75	75	100	100
Integrated tube current (ma)	95	74	66	51	74	70	94	74
% error	5	26	12.5	32	1.5	7.3	5.7	26

distort the curves in this energy range. The table also shows that the agreement is much better for curves taken far from the cathode. This would be expected because the distributions close to the cathode contain an excess of high energy electrons and therefore in this region the planar probe criterion is not as well satisfied. For the distributions found at the port farthest from the cathode the agreement is very good--the error ranging from 1.5 percent to 12.5 percent. This much error is very small when all sources of error are considered. Some of the more obvious sources are:

1. Space potential must be determined. As discussed previously, this is somewhat difficult in general and further complicated here due to the longitudinal field and probe rotation.

2. We tacitly assume that the probe merely rotates about its axis and is not cocked. Actually the o-ring gland

seal allows some other motion besides rotation and linear movement through the seal.

3. The integration involves taking the relatively small difference between two areas as measured with a polar planimeter. This in itself can account for 5 percent error in all cases.

This excellent agreement between integrated values of tube current and measured values certainly supports the supposition that this is a valid means for obtaining electron velocity distributions.

4.3 Neon Distributions

The data presented here will be specified by five parameters:

1. Type of gas
2. Gas pressure (P)
3. Discharge current (I)
4. Longitudinal distance of probe from tube cathode (L)
5. Radial distance of probe from tube wall (R)

We will first look at $g(v_z)$ for v_z parallel to the tube axis. Figure 4.1 shows these distributions at four radial positions in a neon discharge. For these curves the probe was located at the port nearest the cathode (L = 61.5 cm). We see that these distributions are certainly not Druyvesteyn or any other simple function. This was found to be true for all neon curves taken at this port. Figures 4.2 through 4.5 show the same set of curves for the same discharge conditions except the probe has been moved to the port farther from the cathode (L = 69 cm). Also shown on these later curves are the same curves shifted in energy as described previously. (Any discontinuity in the curves at v_z equal to zero was removed by sketching in a

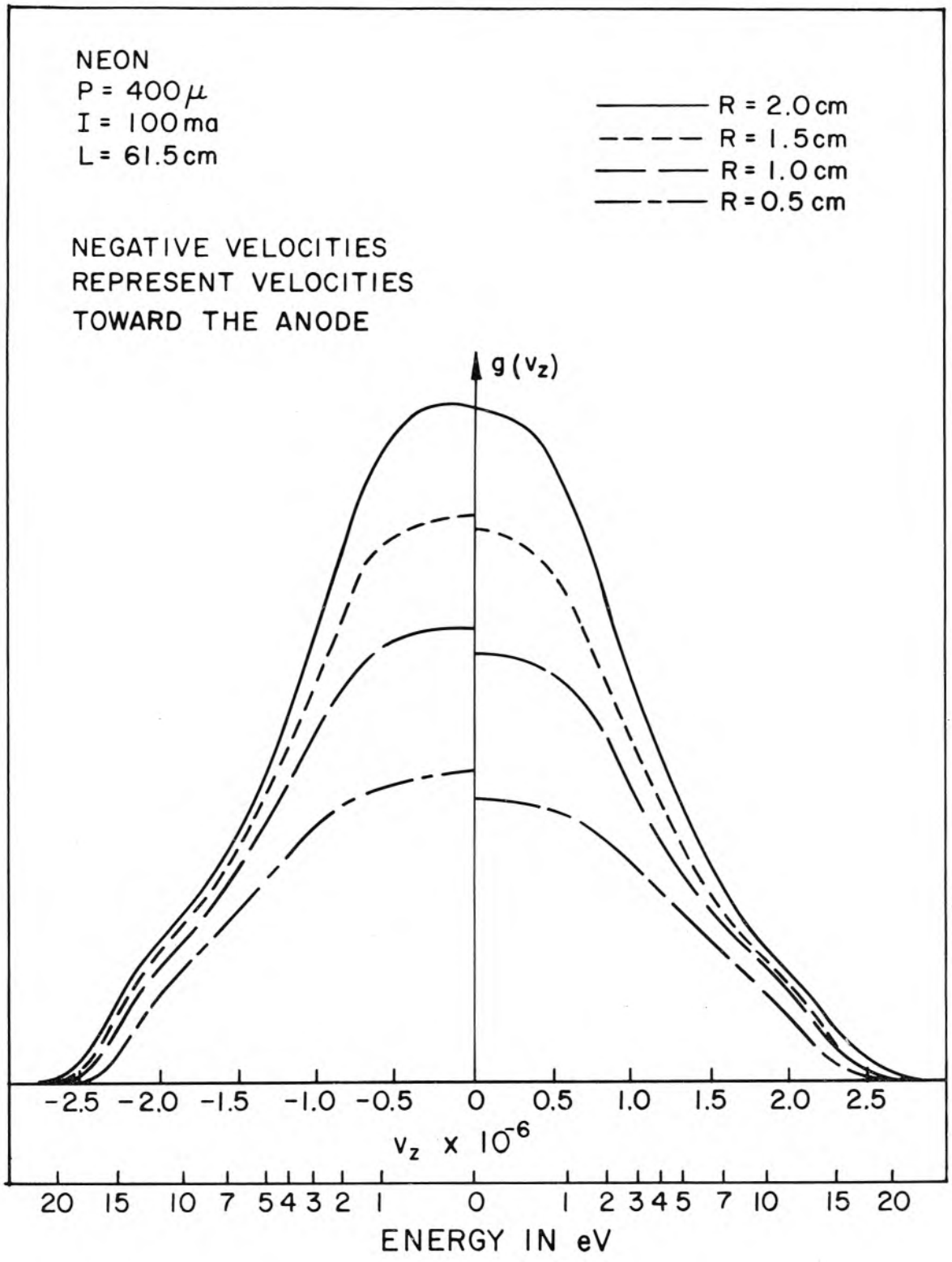

Fig. 4.1 $g(v_z)$ Curves for Neon, Near Cathode End of Positive Column.

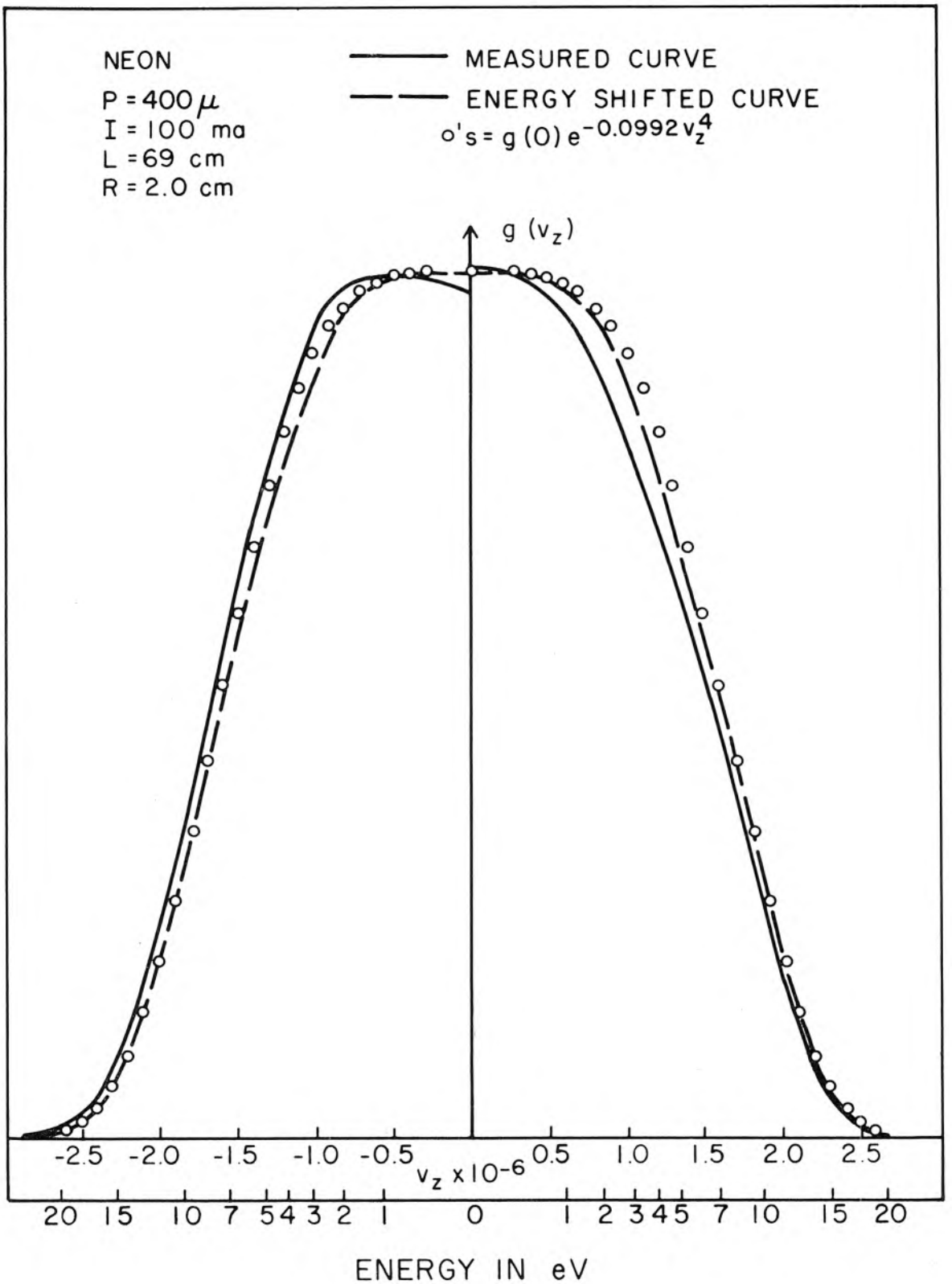

Fig. 4.2 $g(v_z)$ Curve for Neon, Far from Cathode

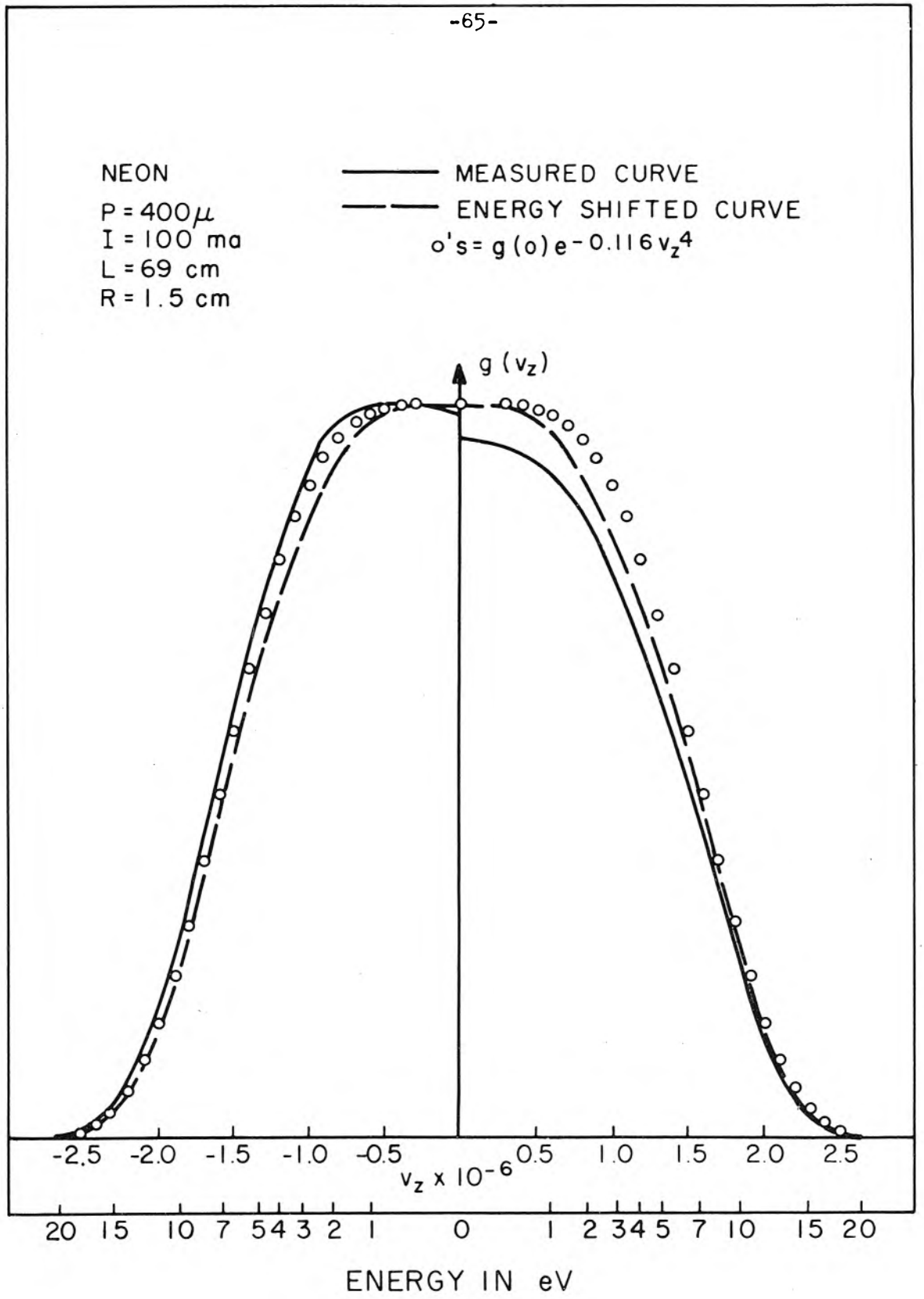

Fig. 4.3 $g(v_z)$ Curve for Neon, Far from Cathode

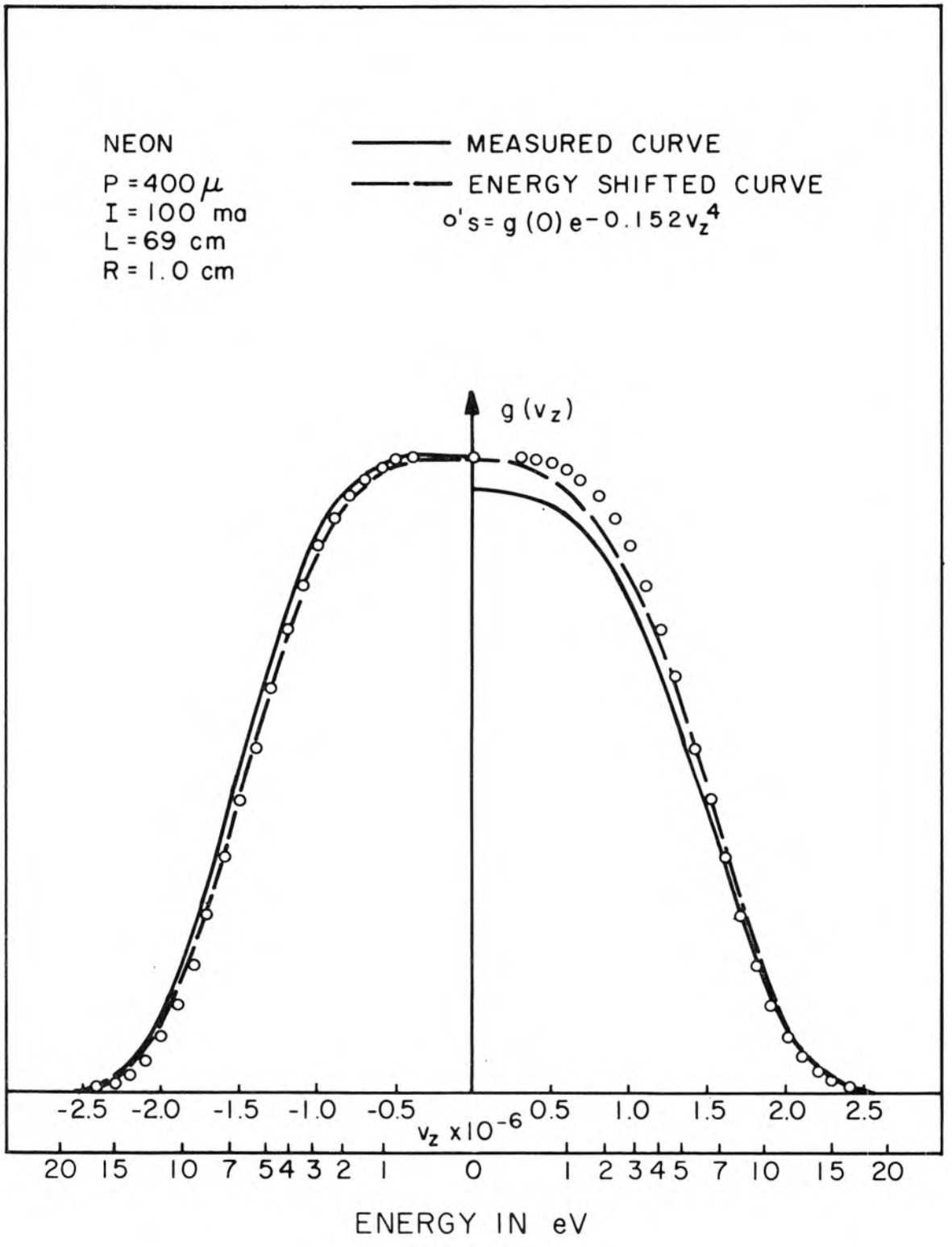

Fig. 4.4 $g(v_z)$ Curve for Neon, Far from Cathode

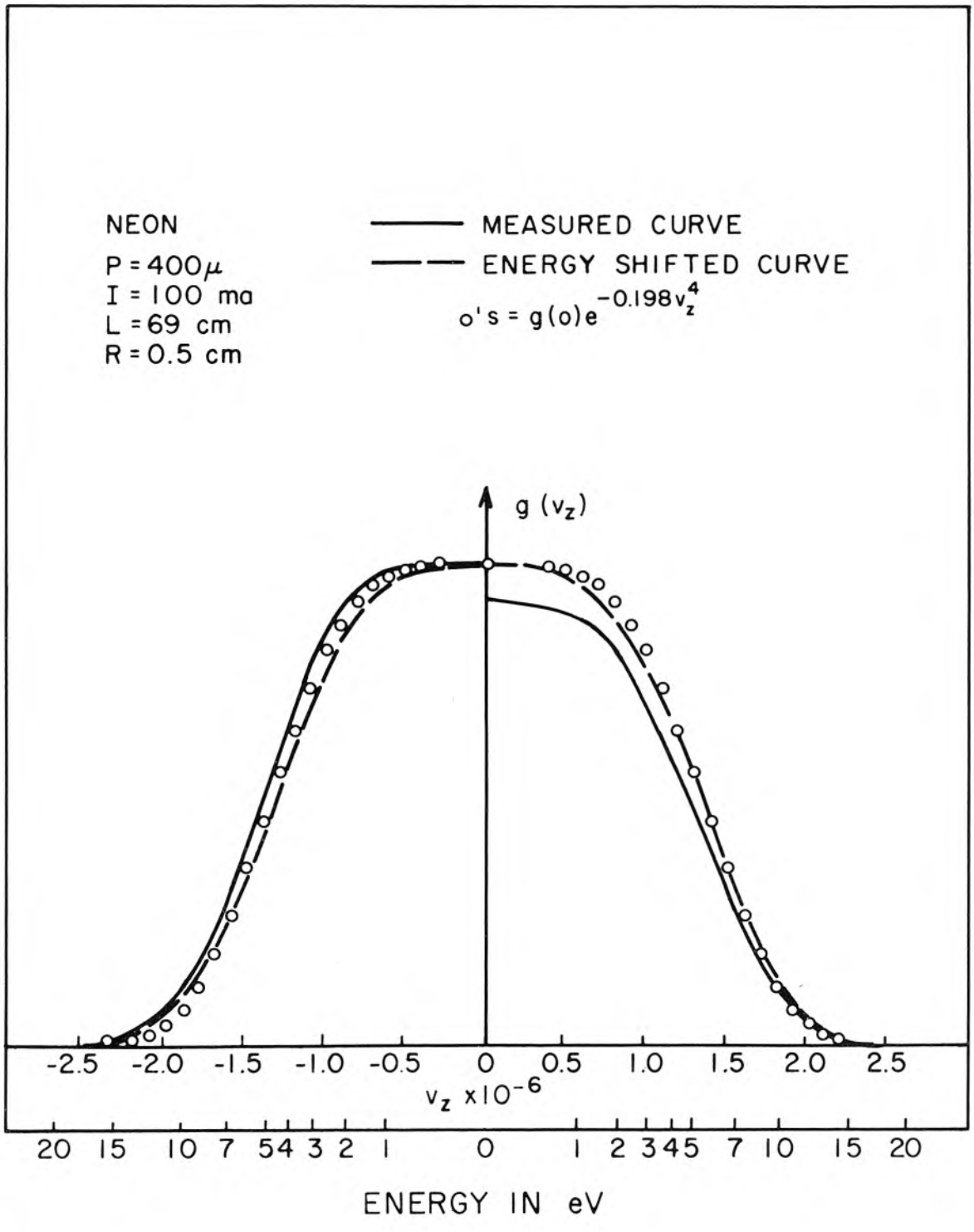

Fig. 4.5 $g(v_z)$ Curve for Neon, Far from Cathode

continuous curve.) It is seen that the shifted curves are very nearly symmetrical about zero. It was found that these symmetrical curves could be fitted very well by a function of the form $Ae^{-b^4 v_z^4}$. This function for $g(v_z)$ corresponds to an $f(v)$ of the form $\frac{2}{\pi} Ab^4 v^2 e^{-b^4 v^4}$. A can be determined from the condition that

$$n = \int_{-\infty}^{\infty} g(v_z)\, dv_z \tag{4.2}$$

which gives $A = \frac{2bn}{\Gamma(\frac{1}{4})}$. Thus we have

$$g(v_z) = \frac{2bn}{\Gamma(\frac{1}{4})} e^{-b^4 v_z^4} \tag{4.3}$$

The mean z-directed energy is

$$\overline{W}_z = \overline{\frac{1}{2} m v_z^2} = \frac{m}{2n} \int_{-\infty}^{\infty} v_z^2\, g(v_z)\, dv_z = \frac{m\Gamma(\frac{3}{4})}{2b^2\Gamma(\frac{1}{4})} \tag{4.4}$$

Figure 4.6 shows this $g(v_z)$ plotted along with a Druyvesteyn distribution which has the same n and mean energy. From this figure we see that the function which fits the neon data has fewer high and low energy electrons than the corresponding Druyvesteyn distribution. This is as expected, since the mean free path for neon decreases with increasing energy.

Curves of the above form were matched to the neon data taken at the port farthest from the cathode (L = 69 cm). The circles on Figures 4.2 through 4.5 represent these calculated curves. It is seen from these figures that the agreement is quite good near the center of

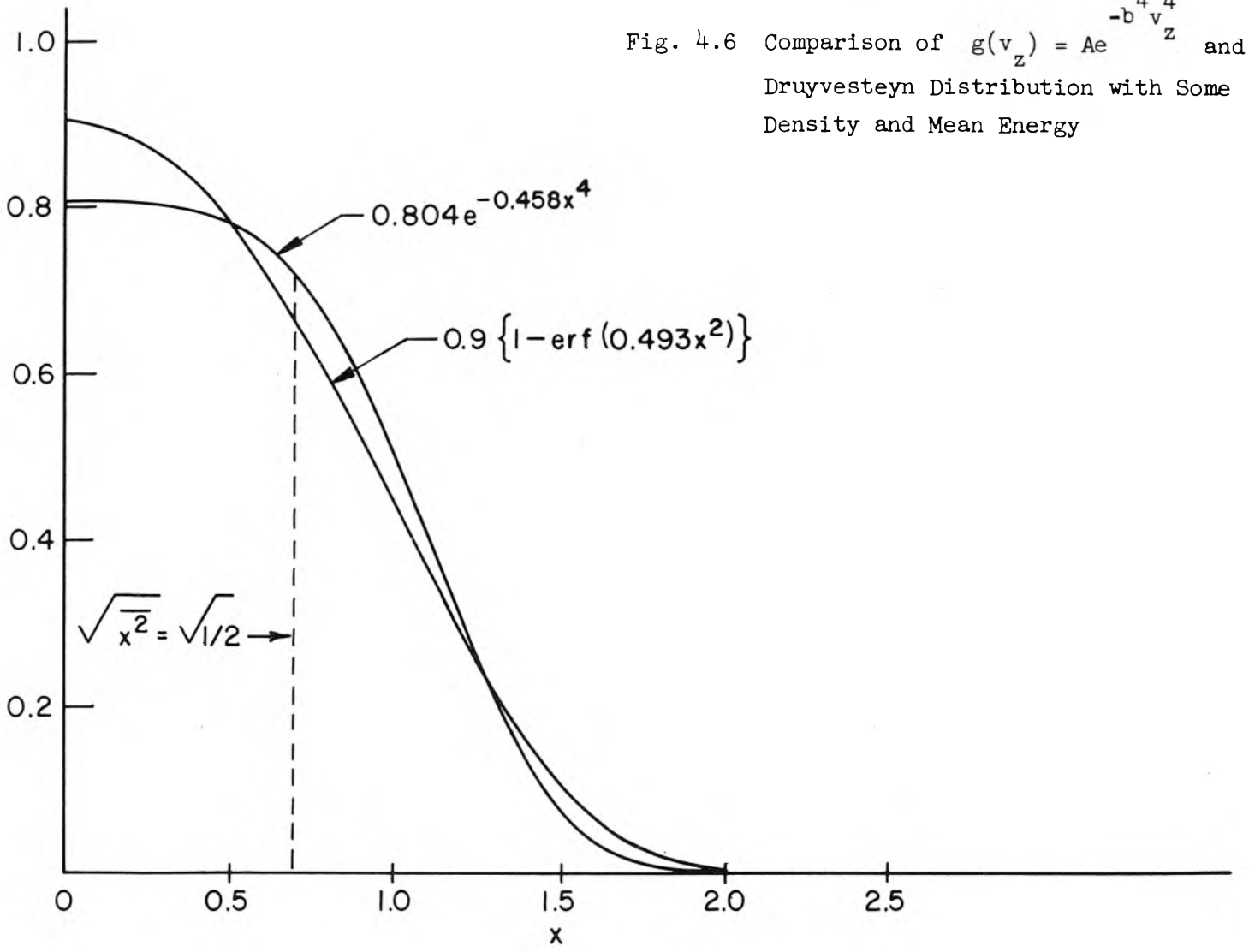

Fig. 4.6 Comparison of $g(v_z) = Ae^{-b^4 v_z^4}$ and Druyvesteyn Distribution with Some Density and Mean Energy

the tube and for energies above seven eV. The disagreement is in a direction to make the measured curves tend toward a Druyvesteyn distribution. The value of b found to match each curve was used to calculate the electron mean energy $(\overline{W}_z)$ as given by equation 4.4.

The simple theory presented in Section 2.3 gives the ion saturation current density as

$$eN_i \sqrt{\frac{kT_i}{2\pi M}} \quad .$$

However, several theoretical treatments, which assume a Maxwellian electron energy distribution, have shown that the fields penetrating from the probe produce an ion flux proportional to $\sqrt{T_e}$ rather than $\sqrt{T_i}$ (2) . To apply these theories to the determination of N_i it is necessary to obtain a number for T_e . Since the measured distributions are not Maxwellian, this value for T_e is somewhat arbitrary. Here we will replace T_e with $\frac{2\overline{W}_z}{k}$. That is, we will assume a temperature which would produce a Maxwellian distribution with the measured mean energy. Since N_i is approximately equal to n , the above considerations lead to the following expression for n_{sat}. (Here we use n_{sat} to denote explicitly that this is the density calculated from the ion saturation current.)

$$n_{sat} \cong N_i = \frac{I_i}{eA} \sqrt{\frac{\pi M}{\overline{W}_z}} \qquad (4.5)$$

---

(2) A review of this work is given by F.F. Chen in the following lecture notes: F.F. Chen, Lecture Notes on Probe Techniques for Plasma Physics Summer Institute, Princeton University (1962).

It should be noted that the experimental ion saturation current was well defined. The probe characteristics showed a constant value of ion saturation current over a range of 15 to 20 volts. This is an indication that the guard ring probe was exhibiting planar geometry, because for any other geometry the current increases with increasing negative probe potential (due to the increase in sheath thickness which increases the effective collecting area of the probe).

Table 4.2 summarizes the measurements made using neon at 400μ pressure with tube currents of 75 and 100 milliamperes. Shown are the values of n_{sat} along with the value of n found by graphically integrating the $g(v_z)$ curves. Also shown are the values of the mean electron energy, the energy shift necessary at low energies to produce symmetrical distributions, and the low energy mean free path times the longitudinal electric field.

The most outstanding things shown in Table 4.2 are

1. The value of n_{sat} is approximately 3.9 times n for the 100 ma curves and 5.5 times n for the 75 ma curves. Since the values of I calculated from the distribution functions agree quite well with the measured values, it is felt that the values of n are accurate. This means that the ion saturation current is even greater than would be expected assuming the ions have a Maxwellian distribution with $T_i = \frac{2\overline{W}_z}{k}$.

2. The energy shift necessary at low energies agrees well with the value of the longitudinal field times the low energy mean free path. As seen in the table, the shift is always greater than the product, but both quantities generally vary in the same fashion. It is seen that

TABLE 4.2

Measured Neon Parameters

Discharge Description	R(cm)	$n \times 10^{-15}$	$n_{sat} \times 10^{-15}$	$\bar{W}_z$(eV)	Energy Shift(eV)	Eλ(eV)
Neon	2.0	4.53	17.5	3.03	0.9	0.67
P = 400μ	1.5	3.71	14.5	2.80	0.8	0.62
I = 100ma	1.0	2.99	9.70	2.45	0.4	0.56
L = 69 cm	0.5	2.02	7.77	2.15	0.7	0.55
Neon	2.0	2.90	Curves were not simple symmetrical curves with energy shift, so these parameters were not found.			
P = 400μ	1.5	2.48				
I = 100ma	1.0	2.08				
L = 61.5cm	0.5	1.47				
Neon	2.0	2.74	15.0	3.03	1.1	0.72
P = 400μ	1.5	2.31	12.5	2.77	0.7	0.68
I = 75 ma	1.0	1.88	9.43	2.47	0.9	0.64
L = 69 cm	0.5	1.24	7.37	2.00	0.7	0.62
Neon	2.0	2.55	See above note			
P = 400μ	1.5	1.77				
I = 75 ma	1.0	1.40				
L = 61.5cm	0.5	0.88				

there is some scatter in the measured energy shift data. This scatter is of the order of tenths of an electron volt. This magnitude of error is not surprising in that the experimental value of this energy shift is directly dependent upon the correct determination of the $V_p = 0$ point of two derivative curves.

The mean free paths used in the above calculations were calculated from the experimental curves giving the microscopic cross section, as

given by R. B. Brode (3).

Having this information we can now see whether the approximations made in the theory section are valid. First, we assumed very low percentage ionization. For gas pressures used in the experiment (0.3 to 0.5 mmHg) the neutral density is of the order of 10^{22} per m^3. Table 4.2 shows that the electron density is of the order of 10^{15} per m^3. The percentage ionization is therefore 10^{-5} so this approximation is valid.

Second, to obtain a Druyvesteyn distribution the "strong field" condition must be met. This condition is

$$\frac{W_\lambda^2 M}{6mW} \gg kT \qquad (4.6)$$

A stronger condition is

$$\frac{W_\lambda^2 M}{kT\, 6mW_{max}} \gg 1 \qquad (4.7)$$

where W_{max} is the maximum electron energy considered. The distribution curves show that a reasonable value for $v_{z_{max}}^2$ is 10^{13}. Using this value for evaluating W_{max} in the left-hand side of the above inequality we obtain $3620 \gg 1$ so the "strong field" condition is met. The value for the electric field used for the calculation is 2×10^2 volts per meter, whereas the measured longitudinal field ranged from 140 to 180 volts per meter.

---

(3) R. B. Brode, Rev. Modern Phys. 5, 257 (1933).

A third necessary check is to determine whether the planar probe criterion is met. This can be written as

$$e^{-\left(\frac{d}{2s}\right)^2 \frac{eV_p}{kT_e}} \ll 1 \tag{4.8}$$

where we have assumed a Maxwellian distribution. To evaluate the left-hand side of this inequality we must first determine s, the sheath thickness. Equation 2.65 gives

$$s = 1.53 \times 10^{-3} V_p^{3/4} \left(\frac{m}{M}\right)^{1/4} |J_i|^{-1/2} \tag{4.9}$$

Substituting the smallest measured values of $|J_i|$ into this expression we obtain

$$s = 5.54 \times 10^{-5} V_p^{3/4} \quad \text{meters} \tag{4.10}$$

Again setting $T_e = \frac{2\bar{W}_z}{k}$ and using $\bar{W}_z = 3\text{eV}$ the inequality becomes

$$e^{-11V_p^{-1/2}} \ll 1 \tag{4.11}$$

Most of the distribution function is obtained for $V_p \leq 25$ volts, and for this value we have

$$e^{-11/5} = 0.11 \ll 1 \tag{4.12}$$

We see that the inequality is met, but not too strongly. This is still quite good when it is remembered that the worst case was taken at all points in determining the planar probe criterion. Also, the assumption

of a Maxwellian distribution with an electron temperature equal to $2\overline{W}_z/k$ leads to a stronger condition than actually needed. The actual distributions have much fewer high energy electrons than the assumed distribution, and it is the electrons with high velocities tangent to the probe surface which cause it to behave in a nonplanar fashion.

We see that the theory developed should be applicable as long as we stay below the excitation potential of neon and take into account the effect of the variation of the mean free path with energy. The first excitation potential for neon is sixteen volts, so most of the distribution function lies below excitation potentials and is therefore not affected by inelastic collisions.

Thus all of the assumptions (except λ = constant) made in the theory section are valid for these experiments and the agreement between the theoretical and experimental distributions is justified.

4.4 Helium Distributions

Figures 4.7 through 4.10 show the measured distribution functions for velocities parallel to the tube axis as found in helium. Curves are shown for the probe located 0.5, 1.0, 1.5 and 2.0 cm from the tube wall. The gas pressure is 1mmHg while the tube current is 75 ma. These curves are typical of all the curves found in helium. There was no functional difference between the curves taken at the port nearest the cathode and the port nearest the anode. This is quite different from the results obtained in neon, but it can be easily understood. In the helium case the positive column extends much farther from the anode (i.e., the dark space is shorter) so that both probe ports were located well within the positive column. In neon this

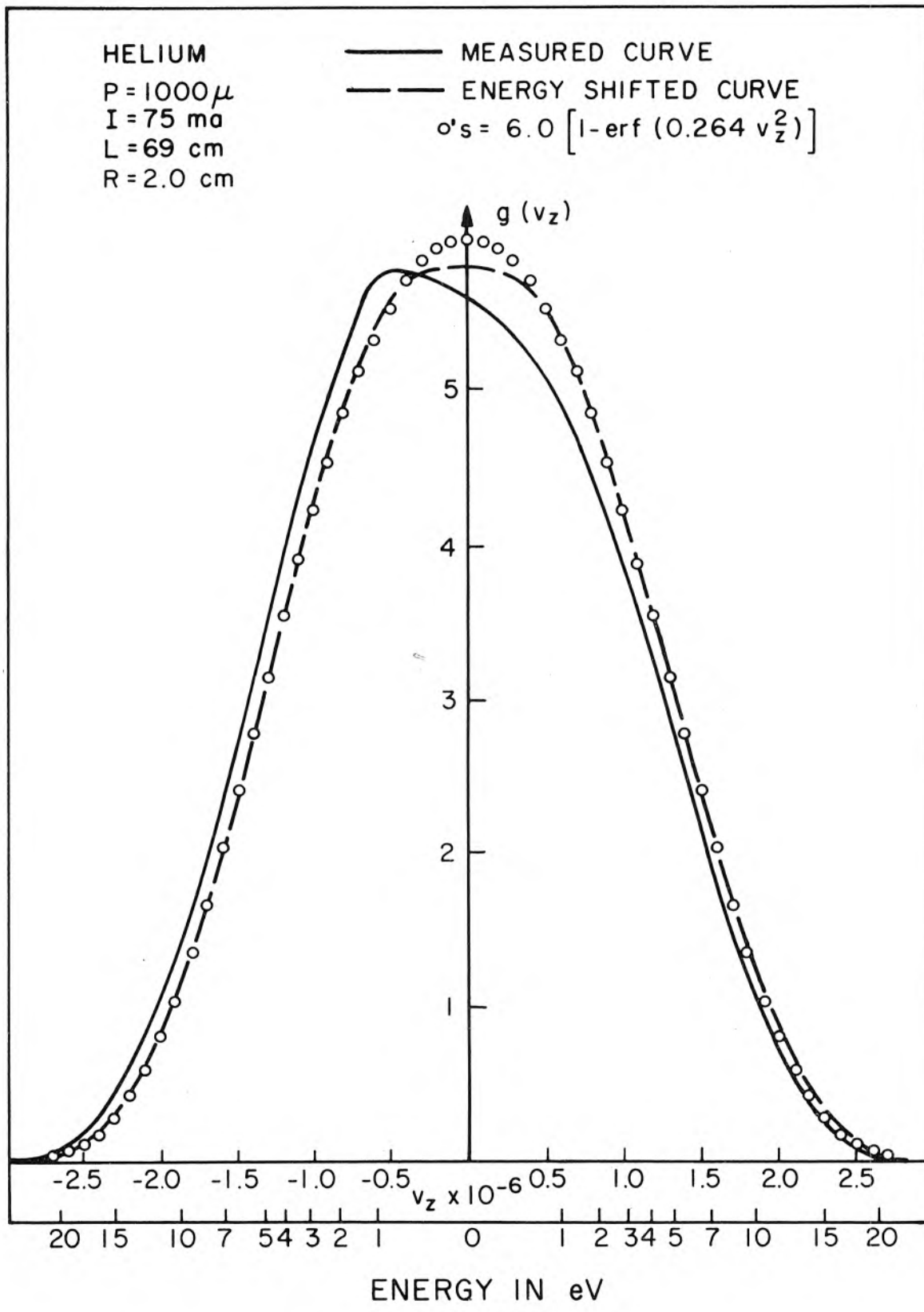

Fig. 4.7 $g(v_z)$ Curve for Helium, Far from Cathode

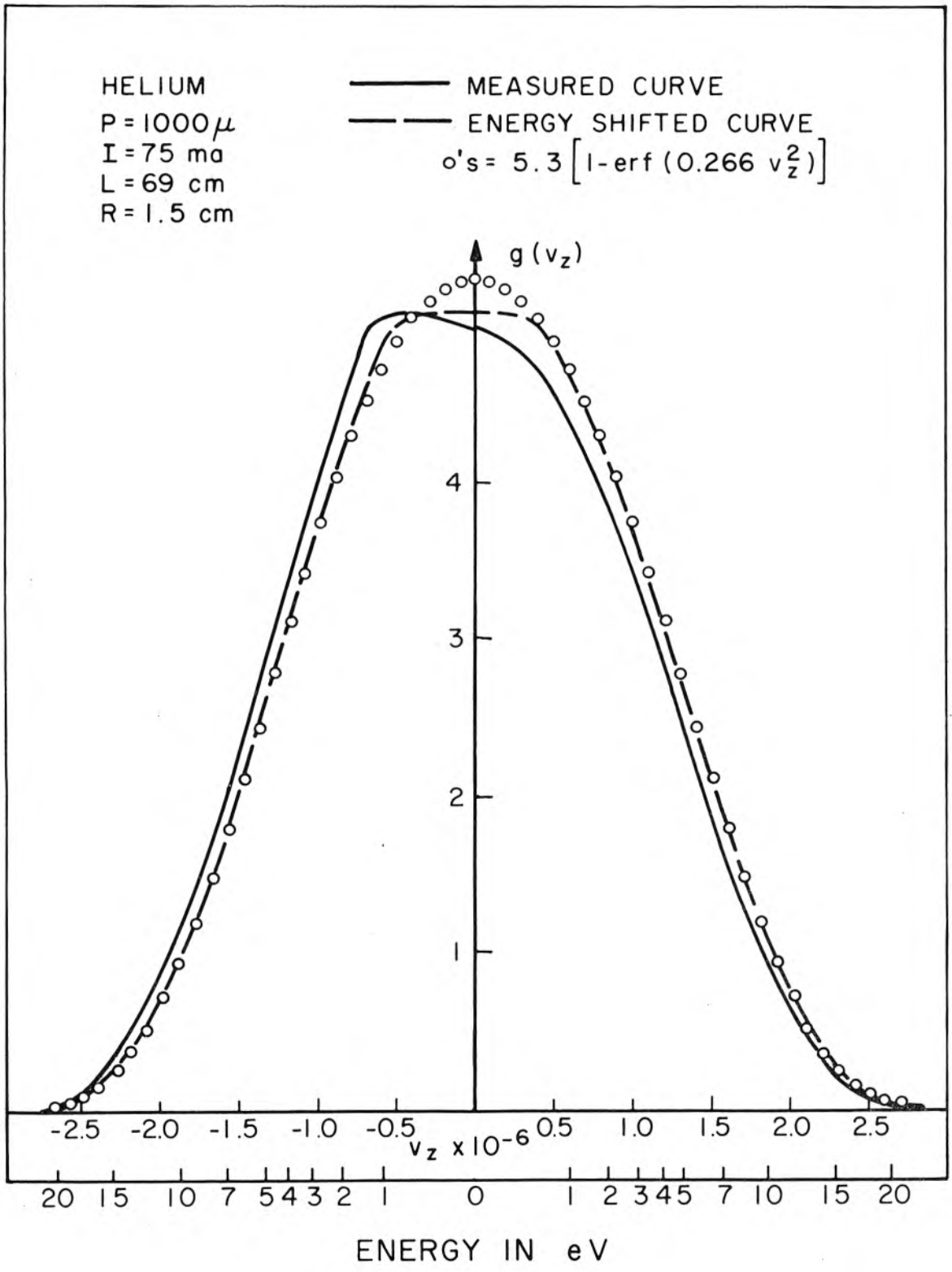

Fig. 4.8 $g(v_z)$ Curve for Helium, Far from Cathode

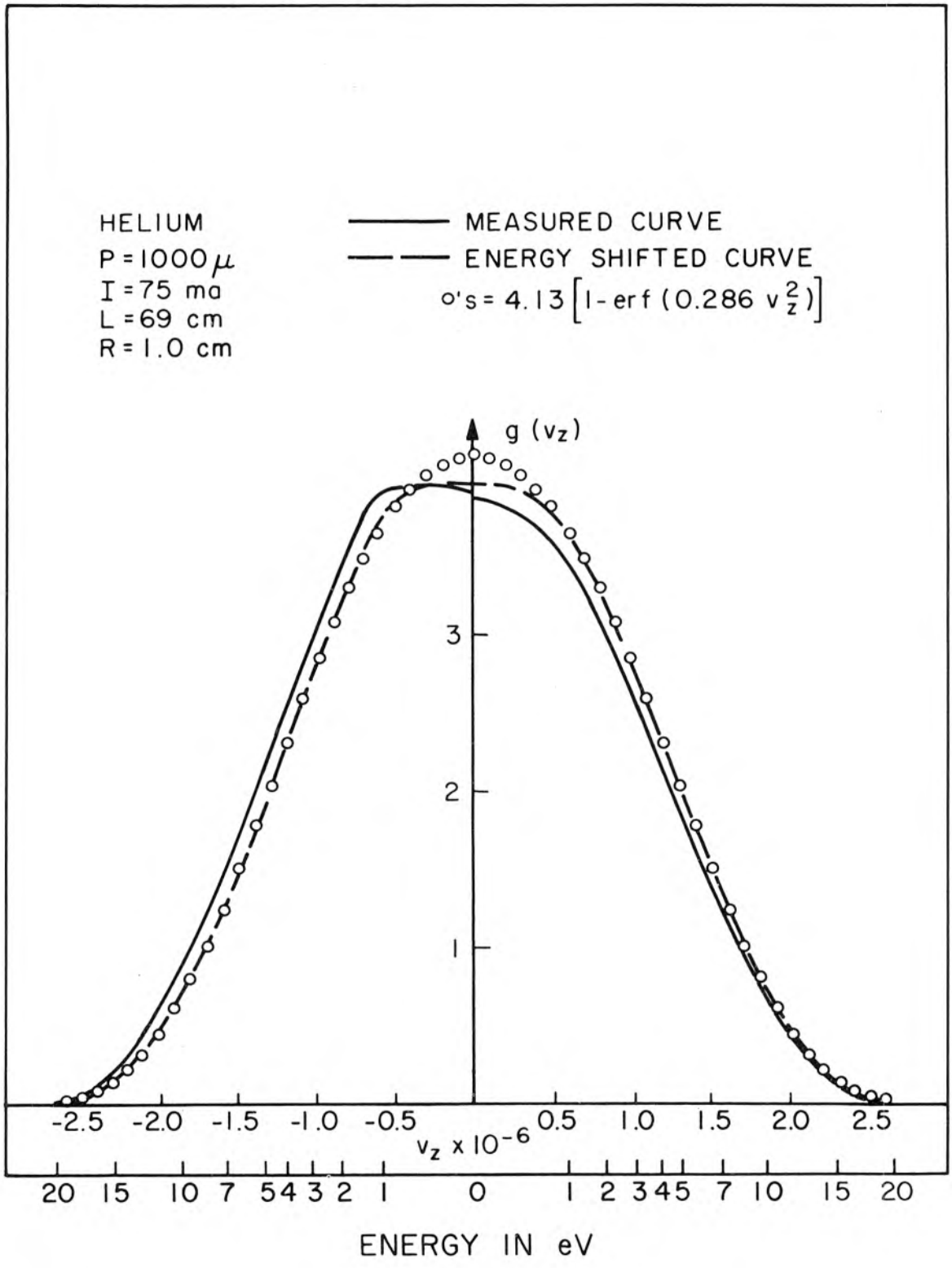

Fig. 4.9 $g(v_z)$ Curve for Helium, Far from Cathode

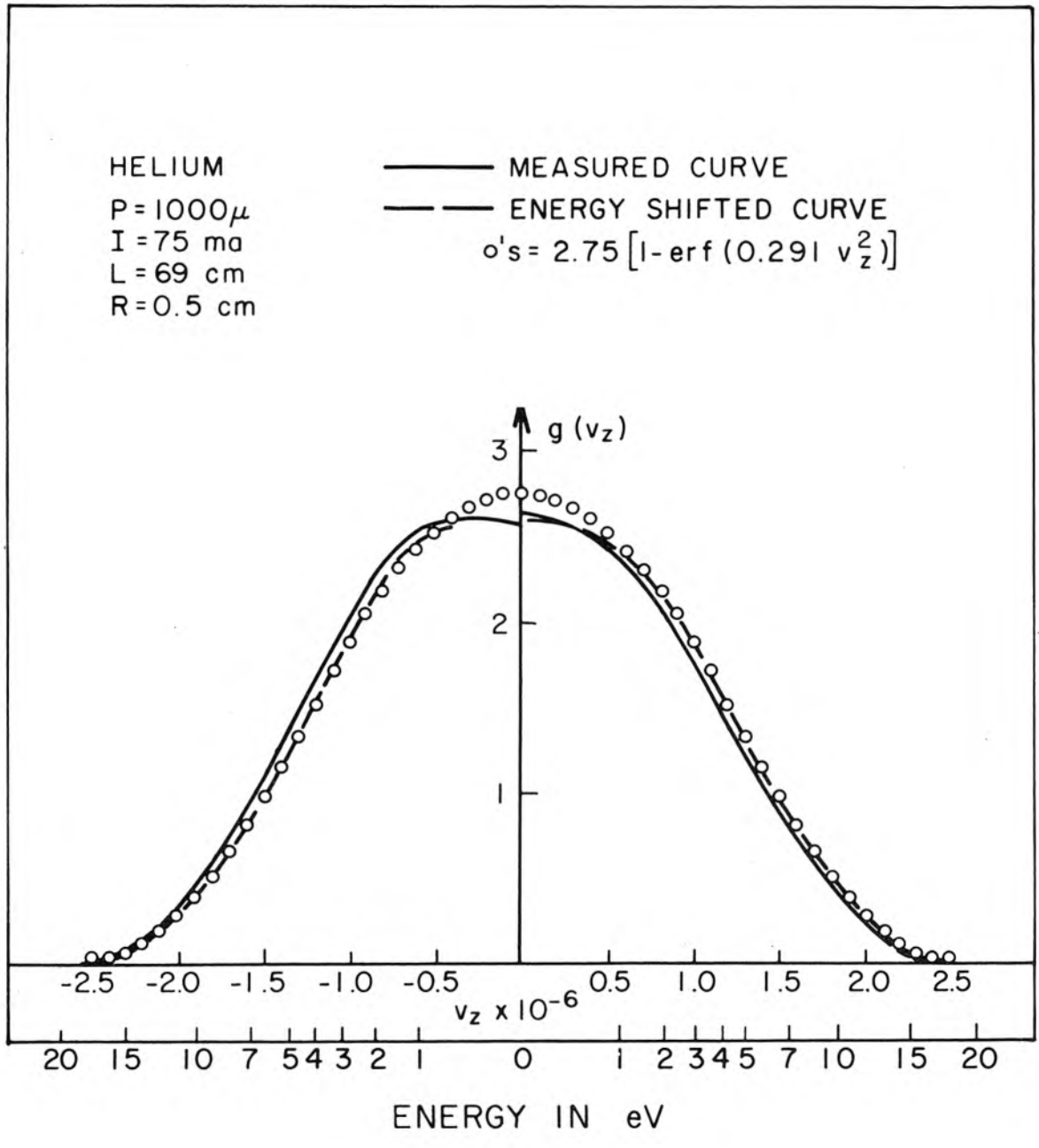

Fig. 4.10 $g(v_z)$ Curve for Helium, Far from Cathode

was not true, as one port was quite close to the cathode end of the positive column.

Also shown in Figures 4.7 through 4.10 are the energy shifted curves as described in the previous section. These shifted curves were found to agree quite well with a Druyvesteyn distribution. The major differences are those expected due to the increase of the mean free path with energy. That is, the measured distributions have fewer low energy electrons and more high energy electrons. However, this excess of high energy electrons exists only up to the first excitation potential (nineteen volts). Above this energy the measured curves lie below the theoretical ones. The circles on these helium curves are best fit Druyvesteyn distributions (i.e., of the form $K[1 - \mathrm{erf}(h^2 v_z^2)]$).

As in the case of the neon curves, the value of h found in matching the experimental curves was used to calculate the mean electron energy. This mean energy was found using equation 2.30 which is

$$\bar{W}_z = \frac{\bar{W}}{3} = \frac{m\Gamma(\frac{5}{4})}{6h^2\Gamma(\frac{3}{4})} \tag{4.13}$$

These values of $\bar{W}_z$ were then used to find n_{sat} as described previously.

Table 4.3 summarizes the helium data for two discharge conditions. It is seen from Table 4.3 that the helium densities (n) lie in the same range as for the previously presented neon data. Also, the mean energies are in the same range, but do not vary as much with radial probe position. Again the same discrepancy exists between n and

TABLE 4.3

Measured Helium Parameters

Discharge Description	R(cm)	$n \times 10^{-15}$	$n_{sat} \times 10^{-15}$	$\bar{W}_z$(eV)	Energy Shift(eV)	Eλ(eV)
Helium	2.0	4.11	21.6	2.67	0.65	0.152
P = 1000μ	1.5	3.60	17.5	2.64	0.55	0.151
I = 75 ma	1.0	2.72	13.9	2.46	0.45	0.149
L = 69 cm	0.5	1.79	9.6	2.41	0.35	0.149
Helium	2.0	3.08	16.7	2.68	0.8	0.152
P = 1000μ	1.5	2.68	15.0	2.52	0.7	0.151
I = 75 ma	1.0	2.06	11.5	2.34	0.6	0.149
L = 61.5cm	0.5	1.37	9.2	2.09	0.5	0.149
Helium	2.0	4.05	23.6	2.96	0.7	0.295
P = 500μ	1.5	3.48	20.1	2.85	0.6	0.295
I = 100 ma	1.0	2.72	16.4	2.75	0.65	0.292
L = 69 cm	0.5	1.83	11.0	2.70	0.45	0.282
Helium	2.0	3.10	20.2	2.49	0.65	0.295
P = 500μ	1.5	2.82	18.7	2.38	0.6	0.295
I = 100 ma	1.0	2.16	14.0	2.41	0.55	0.292
L = 61.5 cm	0.5	1.47	10.7	2.31	0.5	0.282

n_{sat}. The ratio of n_{sat} to n goes from 5.1 to 6.5

The values of the energy shifts necessary to produce symmetrical distributions are a factor of 1.6 to 4.3 greater than the product of the mean free path times the longitudinal fields. The agreement here is not as good as that for neon. However, except for the energy shifts found for L = 61.5 cm, P = 1000μ and I = 75 ma, the qualitative variation of these two quantities with position and discharge

conditions is the same. Again, we can check the validity of the assumptions made in the theory section.

The percentage ionization is the same as in the neon case and thus quite low.

The strong field condition is not met as strongly since the relation contains the mass of the neutral scatterers and in this case the mass is a factor of five less. It is still well satisfied giving $725 \gg 1$ with an assumed longitudinal field of 200 volts per meter. The actual fields were 220 to 230 volts per meter.

The planar probe criterion is met to a higher degree because the sheath thickness is less, being given by

$$s = 4.26 \times 10^{-5} V_p^{3/4} \text{ meters} \qquad (4.14)$$

Thus we see that the assumptions made in the theory section are justified for all of the data presented here.

4.5 Movable Cathode Tube

In the last section it was pointed out that the helium distributions taken at both probe ports were functionally the same. To see whether the electron distributions in helium near the cathode end of the positive column were similar to those found in neon, a tube with a movable cathode was constructed. Since the length of the discharge tube merely altered the length of the positive column, this made it possible to probe continuously along the positive column. This also made it possible to determine whether the field in the positive column was uniform. The latter was of interest because the data reduction

presented previously depends on knowing the longitudinal field accurately, and this field was found by assuming a uniform field between the probe ports.

The movable cathode tube was constructed in the same way as the fixed cathode tubes except that a sliding o-ring seal driven by a threaded rod was provided as shown in Figure 4.11. Since sliding o-ring seals leak when they are moved and also because moving the cathode changed the tube volume and thus the gas pressure, it was necessary to pump out and refill the tube after only slight cathode movement. Thus this tube was only suitable for obtaining a rather limited amount of qualitative data. It did serve its purpose by demonstrating that the distributions in helium do contain an excess of high energy electrons near the cathode end of the positive column. A set of curves plotted versus distance from the cathode is shown in Figure 4.12. It was also found that while the cathode was moved a distance of 8 cm, the difference between the anode potential and the probe space potential varied only five percent. Thus the field was quite uniform over the distance probed.

4.6 Other Properties of Measured Distribution Functions

All of the previous discussion has been concerned with the distributions as a function of the velocity component parallel to the axis of the discharge tube. It will not be necessary to discuss the distributions obtained for azimuthal and radial velocities to any great extent because they fit logically with what was found for the longitudinal velocity distributions.

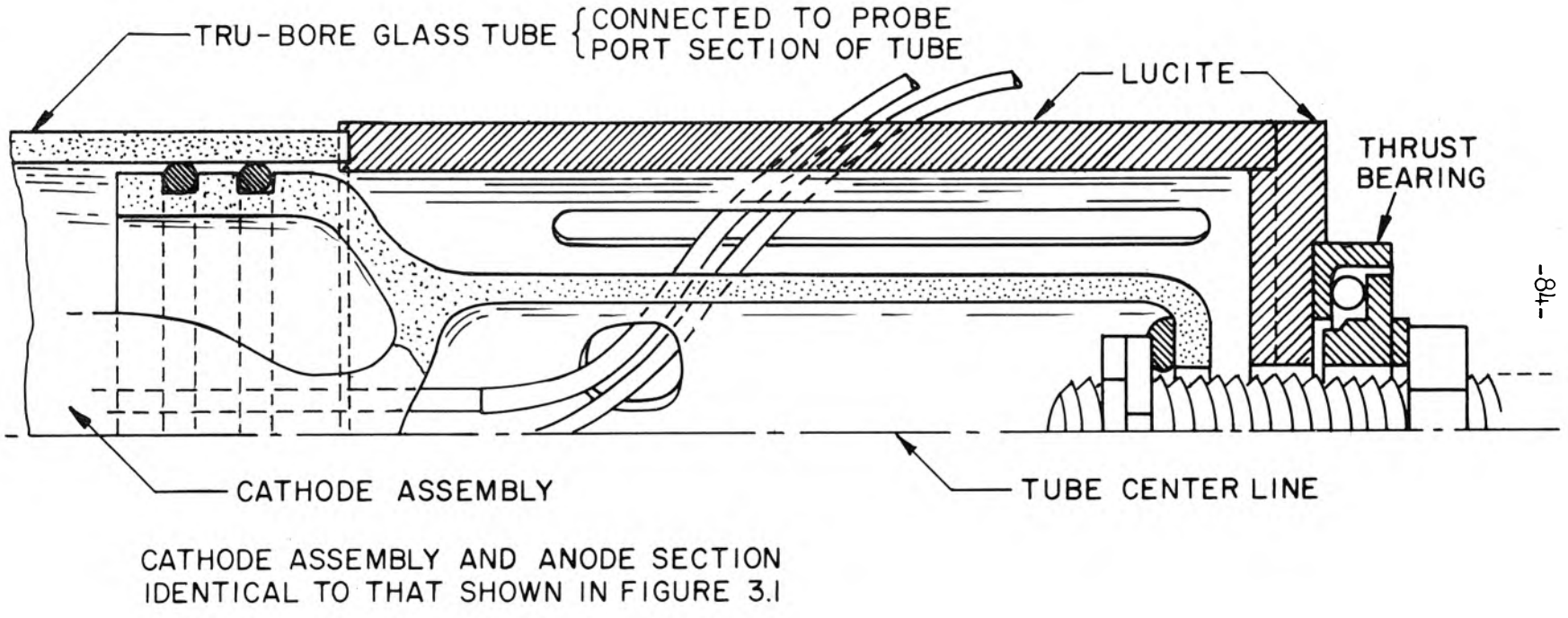

Fig. 4.11 Diagram of Movable Cathode Tube

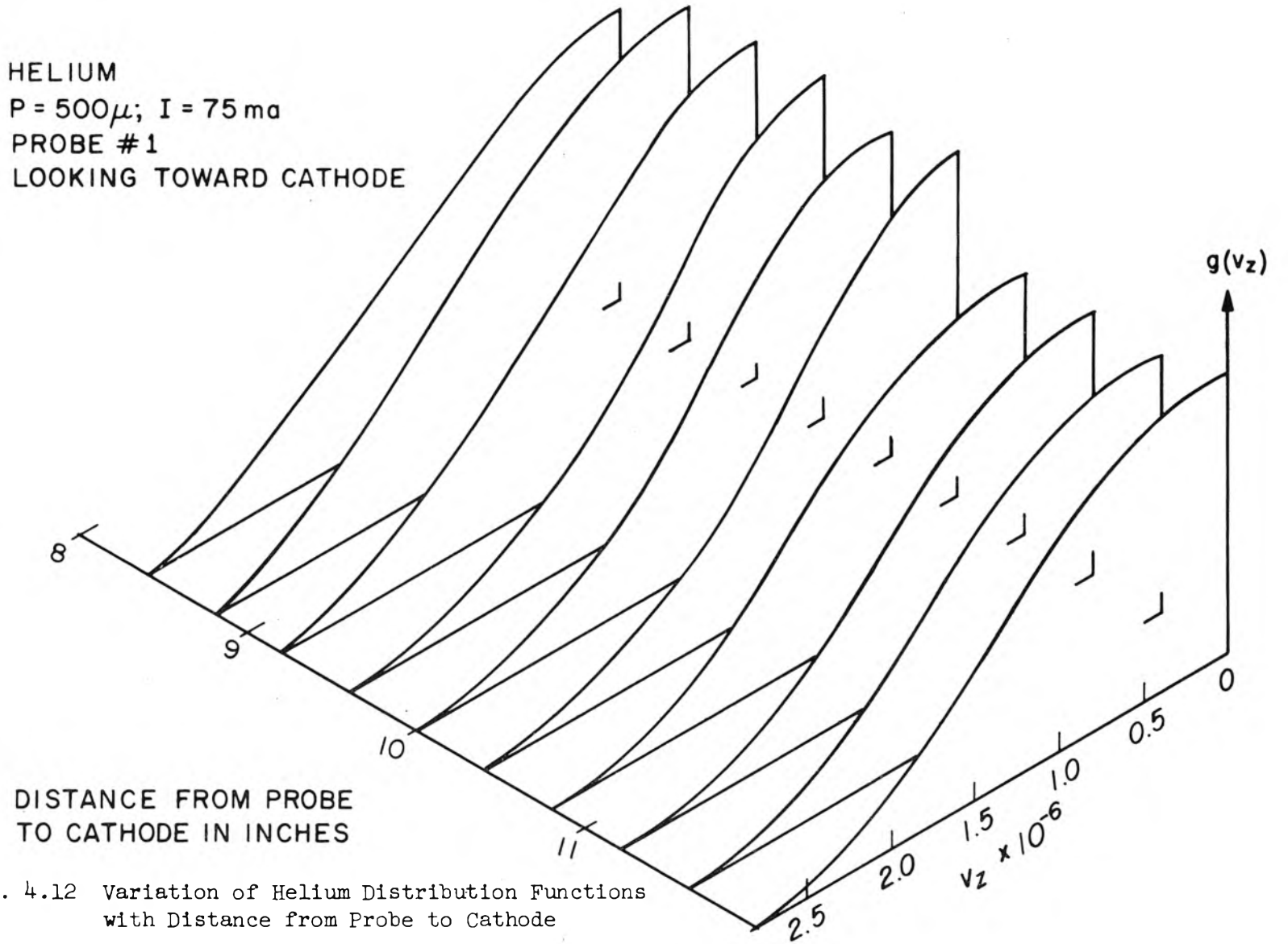

Fig. 4.12 Variation of Helium Distribution Functions with Distance from Probe to Cathode

The distributions involving azimuthal velocities were found to be identical with the energy-shifted longitudinal curves found at the same point under the same discharge conditions. This is as expected, since the cylindrical symmetry of the tube and discharge rules out any azimuthal field which would energy shift these curves.

Since only one-half of the radial distributions was obtained, it was difficult to interpret these curves. However, it was found that these curves had the same form as the energy-shifted longitudinal curves when shifted in energy by the proper amount. The direction and order of magnitude of the necessary shift was in agreement with the measured radial field. This field was found by plotting the radial space potential as determined from probes one or two when they were oriented in an azimuthal direction. The radial field ranged from zero at the center of the tube to approximately 400 volts per meter at 0.5 cm from the tube wall. In most cases the field varied linearly with radius near the tube center. This implies a constant charge density. Simple Gauss' law calculations show that the difference in ion and electron densities necessary to produce the measured fields is

$$N_i - n \approx 10^{12}\ m^{-3} \tag{4.15}$$

Another interesting set of curves is that which shows the percentage of the tube current carried by the various velocity classes of electrons--that is, curves of the difference between $v_z\, g(v_z)$ for electrons moving toward the anode and $v_z g(v_z)$ for electrons moving toward the cathode. Figure 4.13 shows typical curves of this

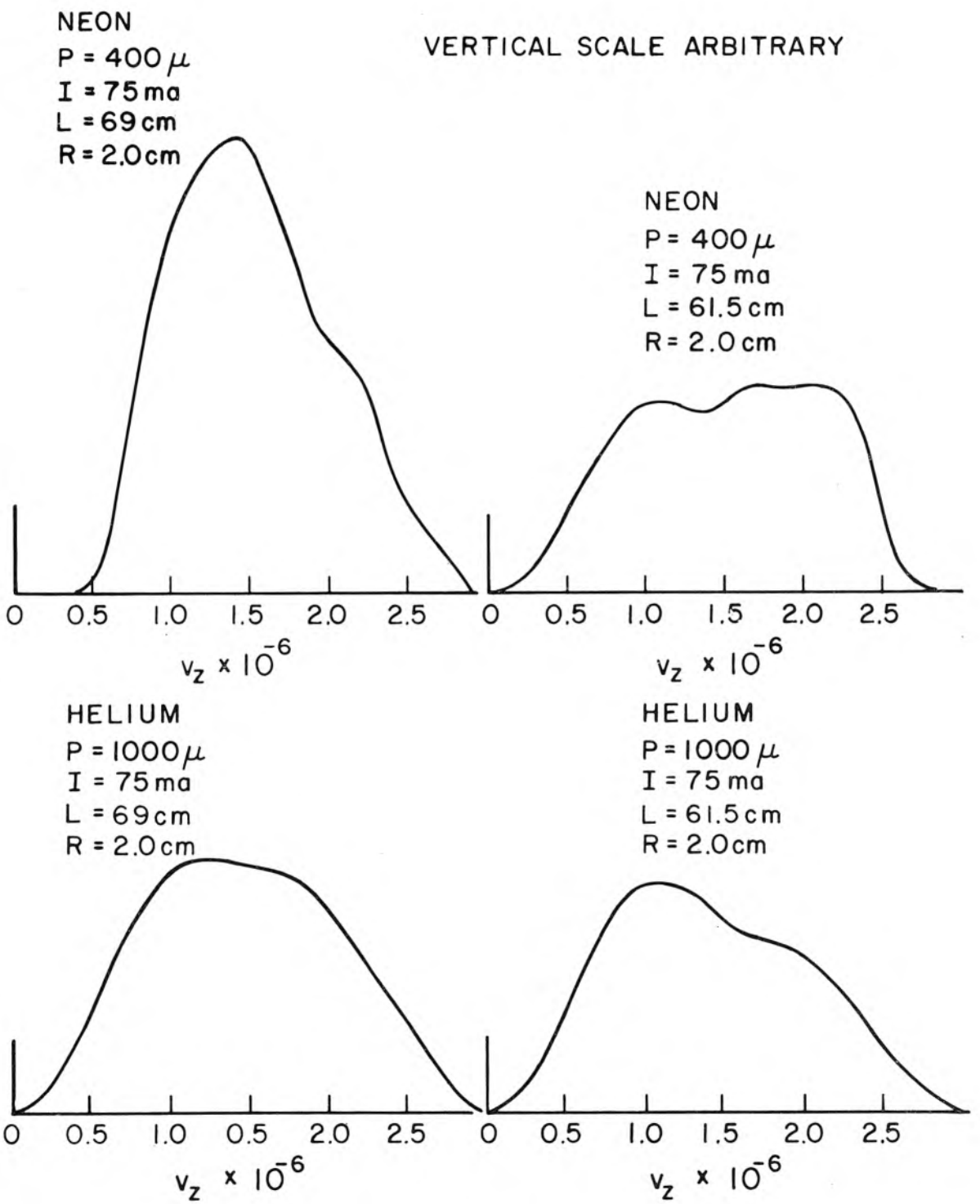

Fig. 4.13 Discharge Current Versus Electron Velocity

type. From these curves we see that in neon near the cathode the tube current is carried equally by a large velocity class of electrons while farther from the cathode the curves are peaked about $v_z = 1.4 \times 10^6$ m/sec. Thus, as we move away from the cathode the high energy electrons become less important in carrying the tube current. This is a graphic display of the change from a directed electron beam at the cathode end of the positive column to an anisotropic Druyvesteyn distribution far from the cathode. Figure 4.14 shows the directional properties of the distributions in neon near the cathode end of the positive column. We see that the anisotropy of the distribution at this position is not merely a general energy shift, but rather a group of electrons directed predominantly from cathode to anode.

The distribution of tube current over the various velocity classes of electrons in helium is similar to that for neon far from the cathode except that the peak is less pronounced. This is shown in Figure 4.13.

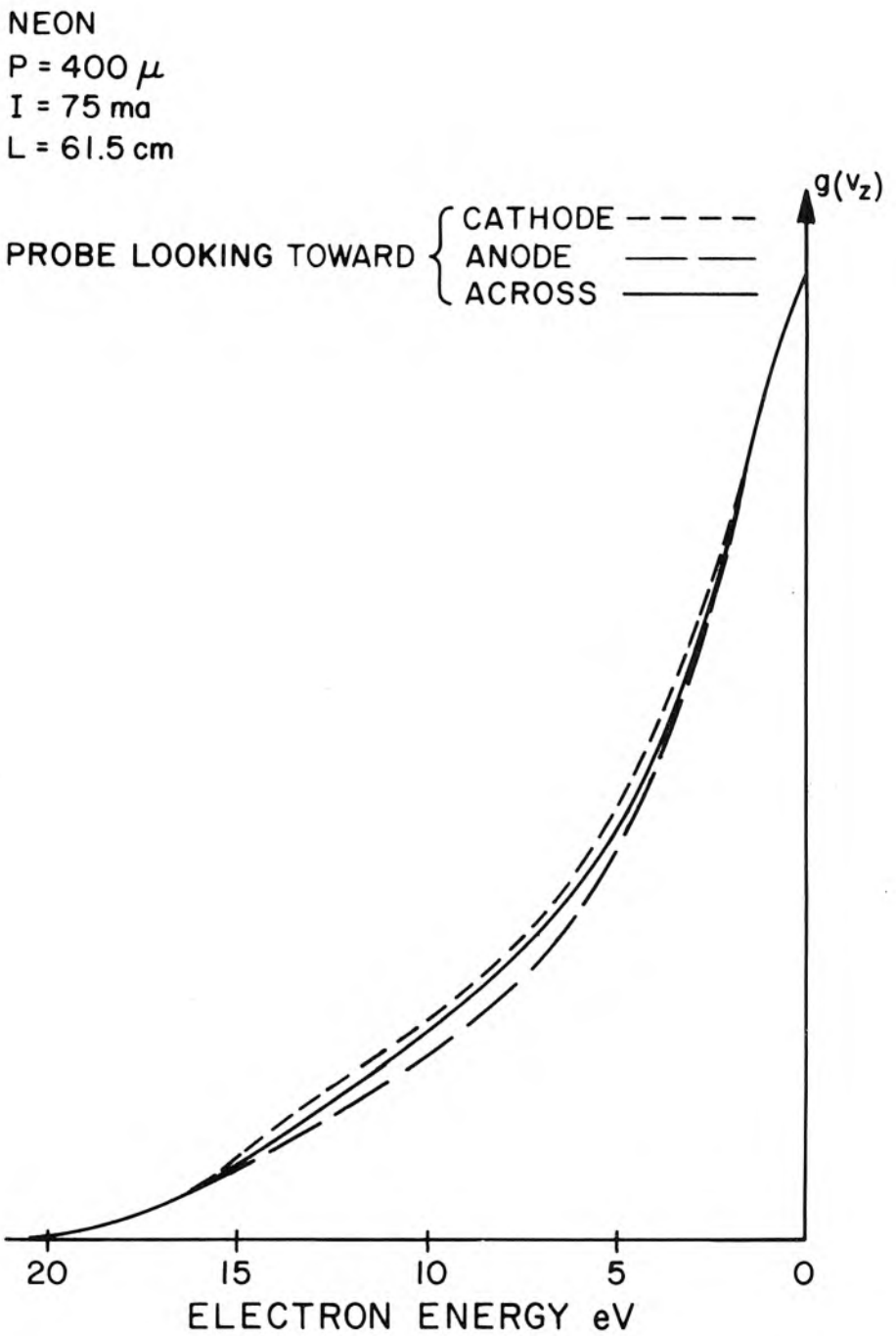

Fig. 4.14 Directional Properties of Neon Distributions near the Cathode End of the Positive Column

V. CONCLUSIONS AND RECOMMENDATIONS

5.1 Conclusions

There are three important conclusions to be drawn from this work:

1. If one is dealing with isotropic distributions, the first derivative of Langmuir probe curves obtained with planar, cylindrical, and small spherical probes all yield the directed velocity distribution $g(v_z)$. It is not necessary to take the second derivative of the probe curves in order to determine electron velocity distributions.

2. For a planar probe the anisotropy of the distribution can be studied using the theory which gives

$$g(v_z) = - \frac{m}{e^2} \frac{\partial J_p}{\partial V_p} \quad .$$

The validity of this technique is demonstrated by the experimental results presented here.

3. The electron distributions in neon and helium hot cathode discharges are nearly Druyvesteyn. Their non-Druyvesteyn nature is due to the high longitudinal electric field (this produces an energy shift of the order of the mean free path times the field strength) and the distortion of the distribution due to the dependence of the mean free path on energy.

The main stumbling block in applying the planar probe theory to the determination of anisotropic distributions is building a planar probe. The excellent agreement between the measured and calculated distribution functions plus the agreement between the tube current

found by integrating $v_z g(v_z)$ and the measured tube current demonstrates that a guard ring probe can be built such that it exhibits planar geometry.

On the negative side this experiment demonstrates that the ion saturation current is not a reliable measure of the electron density. It was shown that the ion saturation current is greater than would be obtained for ions with a Maxwellian distribution whose temperature is $\frac{2\bar{W}_z}{k}$. In fact in these experiments using the simple theory which gives $I_i = AeN_i \sqrt{\frac{kT_i}{2\pi M}}$ leads to a value of N_i which is approximately a factor of 50 too large.

This thesis deals mainly with the specific problem of determining distribution functions using probes. For this reason many of the standard problems in the use of probes are not discussed. Very complete discussions of these are given by Loeb (1), Chen (2), and Francis (3).

5.2 Recommendations for Further Study

The work reported here was done in order to verify that a probe demonstrating planar geometry could be built and, once built, directed electron distribution functions could be measured in detail. It has now been shown that this can be done. A logical extension would be to determine these distributions in other types of plasmas in order to

---

(1) L. B. Loeb, Basic Processes of Gaseous Electronics, (University of California Press, Berkeley 1960) pp.361-370.

(2) F. F. Chen, Lecture Notes on Probe Techniques for Plasma Physics Summer Institute, Princeton University (1962).

(3) G. Francis, Vol.XXII Handbuch der Physik, S. Flügge, Ed., (Springer Verlag, Berlin 1956) p.65.

determine the effects of various external and internal parameters on the distribution functions.

All successful applications of Druyvesteyn's theory for determining distribution functions involve applying small a-c potentials on the probe. It is sometimes argued that these produce oscillations in the probe sheath or plasma proper and thus alter the electron energy distribution. It is possible to measure $\frac{dI_p}{dV_p}$ by applying a small a-c signal to the probe and synchronously detecting the a-c probe current. This could be done and directly compared with measurements made as described here to determine whether or not the a-c signal does alter the energy distributions.

APPENDIX A

In order to determine the form of the collision term which appears in the Boltzmann equation we must first look at the geometry of a binary collision. Figure A-1 depicts such a collision in a frame moving with the scatterer. $\underline{V}(\underline{v})$ are the original velocities of the scatterer (scattered particle) in the laboratory frame, while primes denote final velocities. $\underline{k}$ is a unit vector along the apse line directed toward the scatterer, and b is the impact parameter.

We know energy must be conserved, therefore

$$mv^2 + MV^2 = mv'^2 + MV'^2 \tag{A-1}$$

Writing the initial velocities in terms of the velocity of the center of mass ($\underline{V}_{CM} = \frac{m\underline{v} + M\underline{V}}{m + M}$) and the relative velocity $\underline{u}$ we have

$$\underline{v} = \underline{V}_{CM} + \frac{M}{m+M}\underline{u} \tag{A-2}$$

$$\underline{V} = \underline{V}_{CM} - \frac{m}{m+M}\underline{u}$$

Similarly the final velocities can be written

$$\underline{v}' = \underline{V}_{CM} + \frac{M}{m+M}\underline{u}' \tag{A-3}$$

$$\underline{V}' = \underline{V}_{CM} - \frac{m}{m+M}\underline{u}'$$

Substituting these expressions into A-1 we obtain

$$(m+M)\left\{V_{CM}^2 + \frac{mM}{(m+M)^2}u^2\right\} = (m+M)\left\{V_{CM}^2 + \frac{mM}{(m+M)^2}u'^2\right\}$$

or

$$u = u' \tag{A-4}$$

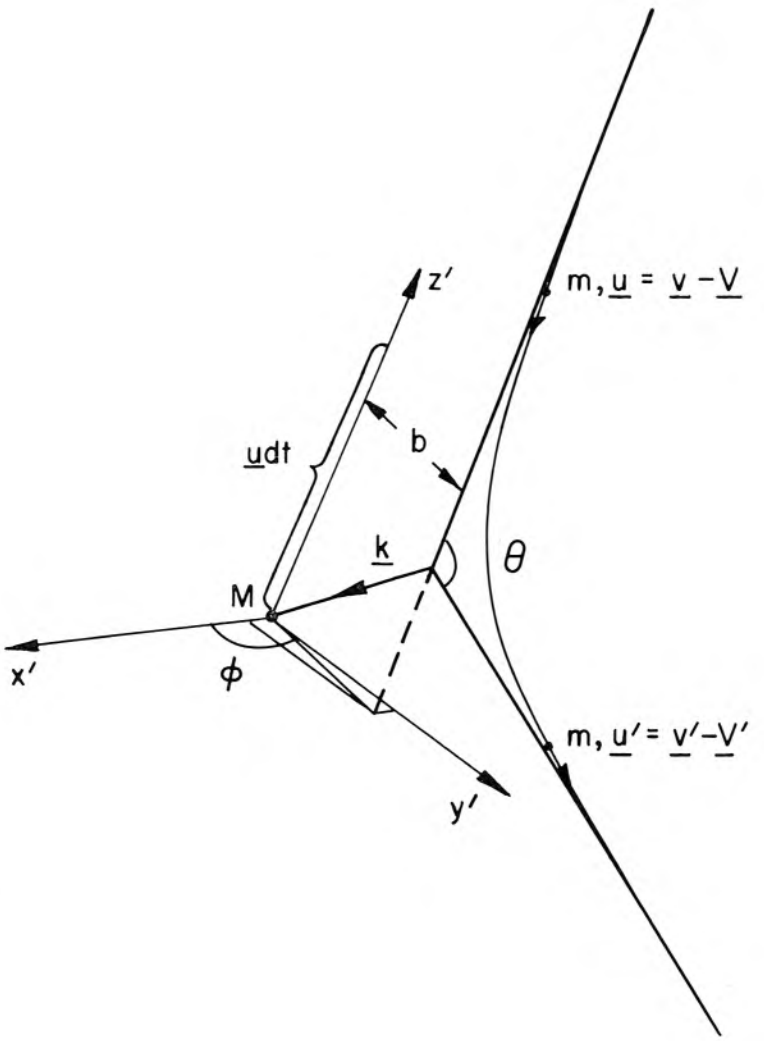

Fig. A-1 Geometry of Binary Collision

Thus we see that in this coordinate system as in the center of mass system the velocity of the particles is constant and merely changes direction.

We are dealing with a central force problem so $\underline{k}$ bisects the scattering angle Θ. Therefore we may write

$$\underline{u} - \underline{u}' = 2\underline{u} \cdot \underline{k}\,\underline{k} = -2\underline{u}' \cdot \underline{k}\,\underline{k} \qquad \text{(A-5)}$$

Using this expression and equations A-2 and A-3 we can write the change in velocity of the particles as follows:

$$\underline{v}' - \underline{v} = \frac{M}{m+M}(\underline{u}' - \underline{u}) = \frac{M}{m+M}(-2\underline{u} \cdot \underline{k})\,\underline{k}$$

$$\underline{V}' - \underline{V} = \frac{m}{m+M}(\underline{u} - \underline{u}') = \frac{m}{m+M}(2\underline{u} \cdot \underline{k})\,\underline{k} \qquad \text{(A-6)}$$

Let us now look at the statistics of the collision. We need an expression for the number of encounters occurring within $\underline{dr}$, in a time dt, between particles of mass m in velocity range $\underline{dv}$ and particles of mass M. Here we assume that dt is short in terms of the time necessary for macroscopic changes in the distribution functions, but long compared to the duration of an encounter.

First we will look at the number of such encounters with particles of mass M in the velocity range $\underline{dV}$, impact parameters in the range b to $b+db$, and ϕ in the range ϕ to $\phi+d\phi$. If only one encounter can occur in a time dt the particle of mass must lie in the volume $bd\phi\ db\ udt$ at the beginning of dt for such an encounter to

occur (see Figure A-1). There is such a volume element for each particle of mass M . The number of volume elements is F $\underline{dV}$ $\underline{dr}$. This gives F $\underline{dV}$ $\underline{dr}$ bdϕ dbudt for the total volume in which a particle of mass m may reside at the beginning of dt in order that this particle undergo one of the above described encounters during the time interval dt. The total number of such encounters will therefore be given by the number of particles of mass m occupying this volume. From the definition of the distribution function the number is

$$fF\ ubdbd\phi\ \underline{dv}\ \underline{dV}\ \underline{dr}\ dt \tag{A-7}$$

This can be written in terms of the microscopic scattering cross section (σ) which is defined as follows:

$$\frac{d\ N_{out}(\theta,\phi)}{dt} \left\{ \frac{\text{number}}{\text{second}} \right\} = \frac{d\ N_{in}(u,b)}{dt} \left\{ \frac{\text{number}}{m^2\text{- sec}} \right\} \sigma(\theta,\phi,u)\ d\Omega \tag{A-8}$$

Noting that we can also write

$$\frac{d\ N_{out}(\theta,\phi)}{dt} = bdbd\phi\ \frac{d\ N_{in}(u,b)}{dt} \tag{A-9}$$

we have

$$bdbd\phi = \sigma(\theta,\phi,u)\ d\Omega \tag{A-10}$$

and equation A-7 can be rewritten as

$$fFu\sigma d\Omega\ \underline{dv}\ \underline{dV}\ \underline{dr}\ dt \tag{A-11}$$

We originally set out to find the total number of encounters irrespective of the velocity of the scatterers and the impact parameter (or scattering angle). This number is merely equation A-11 integrated over all scatterer velocities and scattering angles. Since each of these encounters changes the velocity of the scattered particle, this number represents the number of particles of mass m scattered out of the volume $\underline{dv}\ \underline{dr}$ in a time dt. However, this is just the negative contribution to $\left.\frac{\partial f}{\partial t}\right|_{\text{collision}} \underline{dv}\ \underline{dr}\ dt$. That is,

$$\left.\frac{\partial f}{\partial t}\right|_{\text{collision}} \underline{dv}\ \underline{dr}\ dt = \text{number scattered into } \underline{dv}\ \underline{dr} \text{ in time } dt$$

$$= -\int_{d\Omega}\int_{\underline{dV}} fFu\,\sigma\, d\Omega\ \underline{dv}\ \underline{dV}\ \underline{dr}\ dt \qquad \text{(A-12)}$$

We must now find the number scattered into this volume element. These particles come from inverse encounters--those in which the final velocities are $\underline{v}$ and $\underline{V}$. These encounters involve the following changes from the direct encounters

$$\underline{v}' \rightarrow \underline{v} \qquad \underline{v} \rightarrow \underline{v}'$$

$$\underline{V}' \rightarrow \underline{V} \qquad \underline{V} \rightarrow \underline{V}'$$

$$\underline{u}' \rightarrow \underline{u} \qquad \underline{u} \rightarrow \underline{u}'$$

and $\underline{k} \rightarrow -\underline{k}$

Thus the equations for the change in energy are identical for direct and inverse encounters. That is, for indirect encounters we have

$$\underline{v}' - \underline{v} = \frac{M}{m+M}(-2\underline{u} \cdot \underline{k})\,\underline{k}$$

$$\underline{V}' - \underline{V} = \frac{m}{m+M} (2\underline{u} \cdot \underline{k})\, \underline{k} \qquad \text{(A-13)}$$

showing that the change in velocity for an inverse encounter is equal in magnitude and opposite in direction to that for a direct encounter.

By reasoning similar to that presented above, we can then show that the number of particles of mass m scattered into $\underline{dv}\ \underline{dr}$ in a time dt is

$$\int_{db} \int_{d\phi} \int_{\underline{dV}} f(v')\, F(V')\, u\, b\, db\, d\phi\, \underline{dr}\, dt\, \delta$$

or

$$\int_{d\Omega} \int_{\underline{dV}} f(v')\, F(V')\, u\, \sigma\, d\Omega\, \underline{dr}\, dt\, \delta \qquad \text{(A-14)}$$

where δ is the six-dimensional differential volume element in $\underline{v}', \underline{V}'$ space related to $\underline{dv}\ \underline{dV}$ by the dynamic equations of the encounter, i.e.

$$\delta = |J|\ \underline{dv}\ \underline{dV} \qquad \text{(A-15)}$$

where

$$|J| = \begin{vmatrix} \frac{\partial v'_x}{\partial v_x} & \frac{\partial v'_x}{\partial v_y} & \frac{\partial v'_x}{\partial v_z} & \frac{\partial v'_x}{\partial V_x} & \frac{\partial v'_x}{\partial V_y} & \frac{\partial v'_x}{\partial V_z} \\ \\ \frac{\partial v'_y}{\partial v_x} & \text{etc.} & & & & \end{vmatrix} \qquad \text{(A-16)}$$

It is not necessary to evaluate $|J|$ directly because from the

equations of motion we see that

$$\frac{\partial v_i'}{\partial v_j} = \frac{\partial v_i}{\partial v_j'} \quad \text{etc.} \tag{A-17}$$

therefore $|J|' = |J|$ (A-18)

where $\underline{dv}\ \underline{dV} = |J|'\delta = |J|'\ |J|\ \underline{dv}\ \underline{dV}$

so $|J|'|J| = 1 = |J|^2$ or $|J| = 1$ (A-19)

and the number of inverse encounters is

$$\int_{d\Omega} \int_{\underline{dV}} f(v')\ F(V')\ u\sigma\ d\Omega\ \underline{dr}\ \underline{dv}\ \underline{dV}\ dt \tag{A-20}$$

The collision term can now be written as

$$\left.\frac{\partial f}{\partial t}\right|_{\text{collision}} = \int_{d\Omega} \int_{\underline{dV}} \Big\{ f(v')\ F(V') - f(v)\ F(V) \Big\}\ u\ \sigma d\Omega\ \underline{dV} \tag{A-21}$$

which is the form given in Chapter II.

APPENDIX B

$\underline{E} \cdot \underline{dj}$ (where $\underline{dj}$ is the differential current density) represents the energy given to the electrons (in the energy range W to W+dW) by the field per m^3 per second. Since the field is in the z direction $\underline{E} \cdot \underline{dj} = E\, dj_z$ and

$$dj_z = -\int_{\phi}\int_{\theta_1} ev_z\, fv^2 \sin\theta_1 dv\, d\theta_1 d\phi \tag{B.1}$$

the integral over f_o is zero, so this becomes

$$dj_z = -\int_{\phi}\int_{\theta_1} ev^3 \cos^2\theta_1 \sin\theta_1 f_1 dv\, d\theta_1 d\phi$$

or

$$dj_z = -\frac{4\pi e}{3} v^3 f_1 dv \tag{B.2}$$

giving

$$\underline{E} \cdot \underline{dj} = \frac{-4\pi eE}{3} v^3 f_1 dv = \frac{-4\pi eEv^2 f_1}{3m} dW \tag{B.3}$$

Multiplying equation 2.11 by $4\pi v^2$ and integrating over v we obtain

$$dW 4\pi \int v^2 S_o dv = \frac{-4\pi eEv^2 f_1}{3m} dW \tag{B.4}$$

The right hand side of this equation is just $\underline{E} \cdot \underline{dj}$ so we see that equation 2.11 is directly related to the above energy balance equation which is a statement that the energy gained by the electrons due to the field is lost due to collisions. The energy loss term is a function of

S_o and we would therefore not expect to be able to determine S_o by neglecting the loss in energy of an electron during a collision.

Let us now look at the time rate of change of the z directed momentum for electrons in the energy range W to W +dW due to the electric field. This is $dn\frac{d}{dt}(mv_z)$ which is equal to dn times the force on a single electron. This change in momentum per m^3 per second is therefore

$$-eEdn = -eE \int_{\phi} \int_{\theta_1} f v^2 \sin\theta_1 d\theta_1 dv\, d\phi = -eE 4\pi f_o v^2 dv \qquad (B.5)$$

which can be written

$$-\frac{4\pi eE\, f_o\, vdW}{m} \qquad (B.6)$$

Integrating equation 2.12 with respect to v and then multiplying by $4\pi vdW$ we obtain

$$4\pi vdW \int S_1 dv = \frac{-4\pi eEvdWf_o}{m} \qquad (B.7)$$

Here the f_2 term has been dropped as explained in Section 2.2. The right-hand side of the above equation is exactly the time rate of increase of z directed momentum per m^3 per second for electrons in the energy range W to W+dW due to the electric field. Since we are assuming an equilibrium condition, the left-hand side of B.7 represents the corresponding loss in z directed momentum due to collisions. Because of the large ratio M/m this term, which is a

function of S_1, can therefore be well approximated by neglecting the change in electron energy during a collision with neutral gas molecules.

APPENDIX C

We have shown that f can be written in the form (see equations 2.13 and 2.26)

$$f = f_o + \cos\theta_1 f_1 = A\left\{1 - \frac{6mW}{MW_\lambda}\cos\theta_1\right\} f_o \qquad (C.1)$$

We would now like to show that for the experiment described here

$$\frac{6mW}{MW_\lambda}\cos\theta_1 \ll 1 \qquad (C.2)$$

A stronger inequality is

$$\frac{6mW}{MW_\lambda} \ll 1 \qquad (C.3)$$

This inequality is certainly not met if W is too large or W_λ too small. This means that our assumption that f_1 represents a small perturbation on f_o is not valid for small fields or large energies.

The fields encountered in the experiment described here were of the order of 200 volts per meter. The inequality will be the weakest for helium so substituting numerical values for this case we obtain:

$$W \ll \frac{MW_\lambda}{6m} = 316 \text{ eV} \qquad (C.4)$$

Inelastic collisions become important an order of magnitude below this energy. The theory therefore breaks down long before the second term becomes important, and in the region of interest ($W \leq 30$ eV), f_o is dominant.

Contract Nonr 220(50)

Distribution List

Defense Documentation Center Cameron Station Bldg. 5, 5010 Duke Street Alexandria, Virginia 22314	20
Chief of Naval Research Department of the Navy Washington, D. C. 20360 ATTN: Code 427	2
Commanding Officer Office of Naval Research Branch Office Box 39, Navy 100, FPO New York, New York	1
Commanding Officer Office of Naval Research Branch Office 1030 Green Street Pasadena, California	1
Director U.S. Naval Research Laboratory Washington, D. C. 20390 ATTN: Technical Information Office Code 2027	6